A Light Weight Car Body for High-Speed Trains

Literature study

David Wennberg

Preface

This literature study was carried out during the summer of 2009 as a first step in the PhD project: "*A Light Weight Car Body for High-Speed Trains*". This is a sub-project within "Multi Functional Bodypanels" by the Centre for ECO^2 Vehicle Design at the Department of Aeronautical and Vehicle Engineering at KTH. The economical funding from Vinnova and industry partners Bombardier Transportation, Saab Automobile AB and A2Zound is acknowledged.

Many thanks to my supervisors Sebastian Stichel and Per Wennhage for references and discussions.

Table of Contents

1 Introduction

For rail to compete with other transportation modes there are several factors that have to be taken under consideration, e.g. travel time, ride comfort and price. Advantages that are often pointed out for rail transportation are for example the ability to work or read during travel, that connections often place the passenger in good proximity to city centres and for shorter to intermediate travels, up to 300km when considering the high-speed train X2000, rail transportation is not more time consuming than travel by plane [43]. In our "want(need)-to-be-environmentally-friendly-time" rail also has the benefit of being one of the cleaner travel alternatives.

Here in Sweden the price of train travel does not, however, make it a *clear* choice for travelling, and this is fairly true for any considered distance. To construct a simple comparison travel price and time Stockholm – Malmö and Stockholm – Gothenburg by plane and high-speed train (X2000) are presented in Table 1.

	X2000	**Plane**	**X2000**	**Plane**
Route	*Stockholm – Malmö*		*Stockholm - Gothenburg*	
Price**	850-1050SEK	1000SEK	700-800SEK	1000SEK***
Travel time* **	4h 30min	1h 5min	3h 3-7min	55min

Table 1, travel times and prices between Sweden's three largest cities. Ticket prices from two days notice for Wednesday, 17 June, 2009, economy, one way, adult and only AM tickets.
**Travel time not including any type of transfer from and to airport or train station.*
***Price for X2000 and plane from www.sj.se and www.sas.se respectively*
****Cheapest ticket: 465 SEK, PM ticket*

In the comparison above one should also consider that when looking at total travel times, door to door, train travel will usually gain time on airline travel due to shorter waiting time, no check in required, etc. In [43] B.L Nelldal approximated the average sum of these times to 50min for train and 2h for air travel. As a result, Nelldal showed how travel by X2000 is faster than airline travel for distances up to about 300km. Compared to car travel, train travel (X2000) is faster for distances, door to door, above 150km [43]. The cost of car travel on the other hand depends highly on which car you own. Also, which costs that should be taken under consideration is a matter of opinion. For example should taxes and insurance cost be included in such a comparison? Since, regardless of which transportation method is chosen, a car owner still has to pay this annual cost. I will not try to perform my own cost comparison here, instead state that according to Swedbank*, a used car (98-model**) costs between 19-32SEK/10km (2008), this is including gas, maintenance, parking, devaluation, tax, insurance, etc. Assuming the more expensive cost, 30SEK/10km, a trip to Gothenburg from Stockholm would cost around 1500SEK. By this calculation carpooling two people is as cheap/expensive as taking the train.

** http://www.swedbank.se/ Car models in comparison from Swedbank: Nissan Micra, Toyota Corolla, Volvo 940*
*** In Sweden we have a relatively old car park compared to other European countries, the average age is about 10years per vehicle (not taking account for cars older than 26years) with an average travel distance of 15,000km per year. Statistic vehicle data from: http://www.sika-institute.se/, Swedish Institute for Transport and Communications Analysis, http://www.vv.se, the Swedish Road Administration and http://www.konsumentverket.se, the Swedish Consumer Guide*

The high-speed train X2000 is allowed to run at speeds of 200km/h. If one looks at the travel time for Stockholm – Gothenburg, the average travel speed is 150km/h. Throughout Europe and Asia there are several high-speed train lines which allow for increased speeds in comparison to the X2000 lines in Sweden. This is due to several factors, but for the fastest lines new, dedicated, high-speed lines are often constructed. This requires large infrastructure investments which according to [37] are in the range € 10-50 million (2008) per line kilometre. Another solution is to run at higher speeds on the existing track, which in curved sections requires tilting of the car body, e.g. X2000, to maintain good ride comfort. The typical high weight of rail vehicles in combination with the desired high-speeds puts high stresses on the track, especially in curved sections, resulting in increased maintenance costs.

In the Green Train project a high-speed train is being developed for the Scandinavian market. The spotlight has so far been on running gear and motor technology. The objective of the this PhD project, of which this literature study is the first part, is to look at available light weight car body designs focusing on modern sandwich and composite techniques that can lower the overall weight of the train car body. Other benefits from sandwich design are for example thinner walls, which would increase space in the cabin, possibly allowing 3+2 seating, which would benefit operators, which in turn could benefit ticket prices. A lower weight can also benefit other subsystems, e.g. suspension and brakes, and decrease the overall energy consumption of the rail vehicle. Sandwich design also results in a multifunctional panel design, i.e. the possibility to combine several properties into a single unit, for example sound reduction, thermal insulation, strength and stiffness, thus reducing the number of parts for assembly.

This study furthermore covers design criteria available for passenger rail vehicles and the concept and effects of sandwich construction.

Focus in this study is mainly from a mechanical point of view, however, keeping in mind other important boundary conditions.

2 Concept of Sandwich structures

A sandwich structure consists of three main elements, two outer faces, or skins, and a centre core as shown in Figure 1. The outer faces typically consist of a stiffer, higher density material in comparison to the inner core. Practically any structural material can be used for the faces depending on the purpose of the sandwich construction.

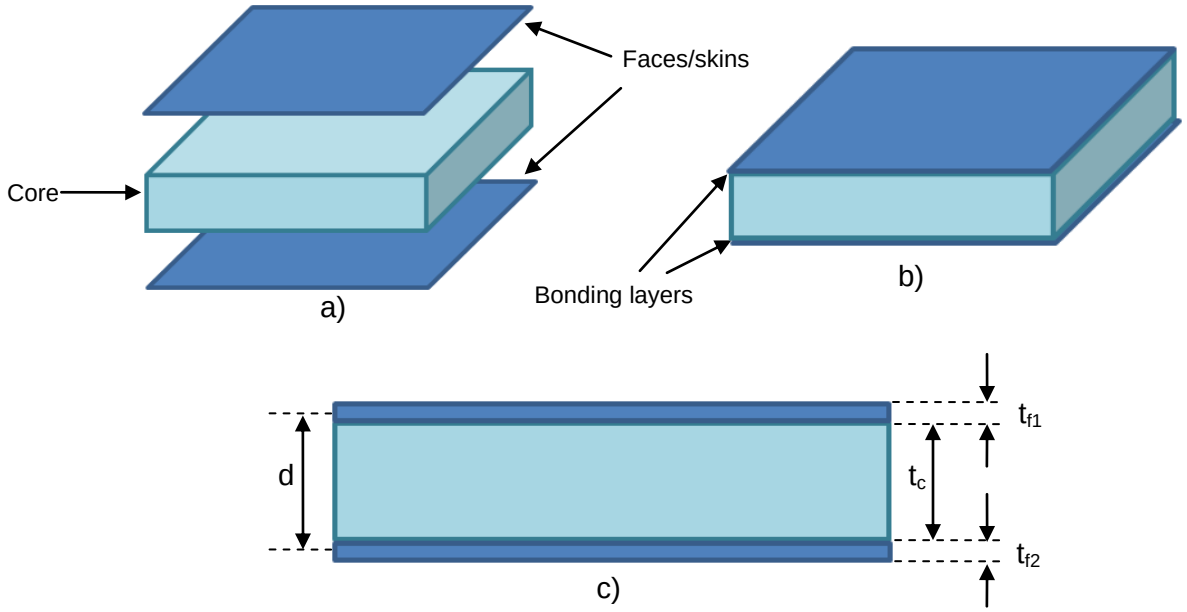

Figure 1, typical sandwich structure
a) sandwich elements
b) bonded structure
c) side view of the sandwich structure

The appellations used in Figure 1, i.e. *c*, *f1* and *f2*, stand for core and first and second face respectively. The same nomenclature will be used to distinguish between different core- and face properties. The face materials are commonly sheet metals or composites while the core materials are usually of lower density materials such as balsa wood, honeycomb structures or polymer foams. There is, however, an almost endless amount of combinations and materials that can be used in sandwich construction and each have their own specific benefits and weaknesses.

The sandwich structure functions in a similar manner as an I-beam in bending, the outer faces are there to withstand the compressive and tensile stresses much like the flanges of an I-beam and the centre core resists most of the shear stresses. To better explain the mathematics in the mechanical behaviour of a sandwich structure some basic equations for beam bending are defined below in accordance with Figure 2 which illustrates a solid beam of length *L* bent to a radius of curvature *ρ*.

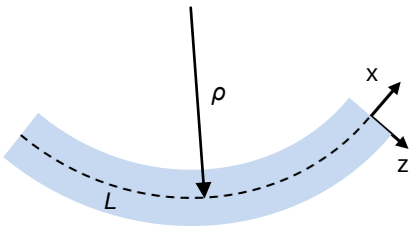

Figure 2, a beam of length *L*, bent to a radius of curvature *ρ*.

The strain in the beam is than by definition

$$\varepsilon_x = \frac{\Delta L}{L} = \frac{(\rho + z)\theta - \rho\theta}{\rho\theta} = \frac{z}{\rho} \quad (1)$$

Here θ is an arbitrary angle giving a certain arc length of the curved beam at $z = 0$ and ΔL is the change in arc length at a certain z-coordinate in the beam, cf. Figure 2. The direct stress in the beam is given by Hooke's law as

$$\sigma_x = E\varepsilon_x = \frac{Ez}{\rho} \quad (2)$$

where E is the Young's modulus of elasticity, which is constant throughout the beam in this example. The required bending moment, M_x, to bend the beam to the specific radius of curvature is then [3]

$$M_x = \int \sigma_x z dz = \frac{E}{\rho}\int z^2 dA \quad (3)$$

The integral in eq. (3) is defined as the moment of inertia for a cross section with respect to the y-dir in Figure 2 and is from now on written as I_y. This gives the following expression for the bending moment

$$M_x = \frac{EI_y}{\rho} \quad (4)$$

By combining eq. (1), (2) and (4) we establish

$$\sigma_x = \frac{M_x z}{I_y} \quad (5)$$

$$\varepsilon_x = \frac{M_x z}{I_y E} \quad (6)$$

By utilising the definition of the flexural rigidity of a solid, rectangular, beam as the product of the elasticity modulus, E, and the moment of inertia, I_y [2],

$$D = EI = E\int z^2 dA \quad (7)$$

the strain and stress, ε_x and σ_x, can now be rewritten as

$$\varepsilon_x = \frac{M_x z}{D} \quad (8)$$

$$\sigma_x = \frac{M_x z E}{D} \quad (9)$$

According to eq. (8) and (9), both the strain and stress vary linearly in the *z* direction throughout the beam with a constant Young's modulus.

With these equations established we can now look at the bending case shown in Figure 3. The stresses and strains vary somewhat differently when looking at a sandwich structure. The two faces can be compared to two solid beams separated by a core with a different elasticity modulus. In eq. (7), the flexural rigidity calculation, the elasticity modulus must be placed inside the integral, since the modulus varies along *z*,

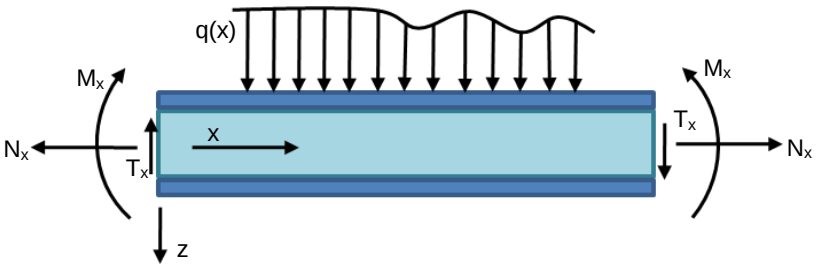

Figure 3, bending of a sandwich structure
z = 0 at centroidal axes of beam

$$D = \int Ez^2 dA \qquad \textbf{(10)}$$

By using the nomenclature in Figure 1, the bending case in Figure 3 and assuming that $E_{f1} = E_{f2} = E_f$, $t_{f1} = t_{f2} = t_f$, the core elasticity modulus is E_c we can write the flexural rigidity of the sandwich structure as [2]

$$D = \int Ez^2 dA = \frac{E_f t_f^3}{6} + \frac{E_f t_f d^2}{2} + \frac{E_c t_c^3}{12} = 2D_f + D_0 + D_c \qquad \textbf{(11)}$$

Here, in accordance with Figure 1, $d = t_c + t_f$. For this 2-dimensional case the flexural rigidity is per unit of length in the y-dir, cf. Figure 3. The first term on the right-hand side of eq. (11) represents the flexural rigidity of the two faces bending about their own centroidal axes'. The second term represents the rigidity of the faces bending about the centroidal axes of the entire sandwich beam while the last term represents the flexural rigidity of the core. The contributions to the total stiffness from the three terms on the right hand side of equation (11) are illustrated in Figure 4 and Figure 5.

Thickness:	d	2d	4d
Flexural rigidity:	1.0	~12	~48
Weight:	1	~1	~1

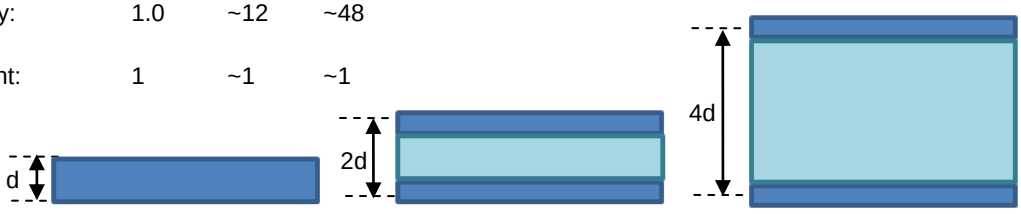

Figure 4, flexural rigidity of three different beams. The left beam is a solid beam while the sandwich beams have face thickness of
$t_f = d/2$
This results in the same amount of face material for each beam.

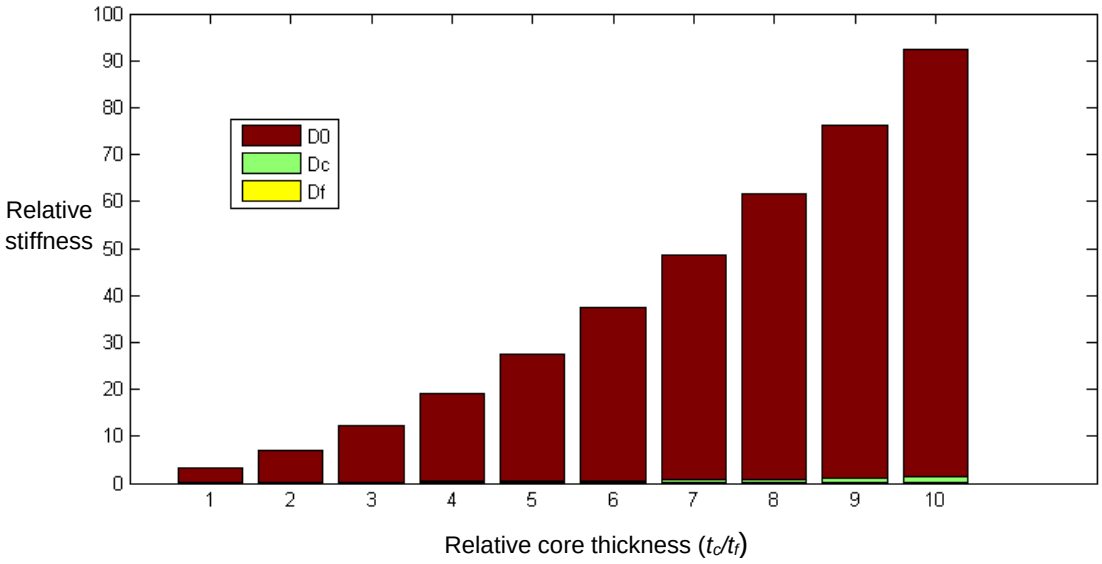

Figure 5, Relative stiffness of a sandwich structure in comparison to a solid beam with Young modulus equal to that of the faces and thickness equal to $2t_f$. Core Young modulus at 1% of face modulus. The different coloured bars represent the different stiffness contributions in eq (11)

Here one can observe the importance of the bonding layer between the faces and core, the contribution from D_c is only just visible in Figure 5 while the contribution from D_f is too small to be distinguished with the current scaling. If the faces are not bonded to the core the term D_0, the red bars in Figure 5, would vanish. The faces and core would only bend around their respective centroidal axes'.

By assuming that sections of the beam remain plane and perpendicular to the centroidal axes of the beam, i.e. perfect bond between face and core, the strain is still defined as in eq. (8). The stresses are then calculated by multiplying with the appropriate elasticity modulus as shown below (coordinates according to Figure 3).

$$\sigma_f = \frac{M_x z E_f}{D}, \qquad \frac{t_c}{2} < |z| < \frac{t_c}{2} + t_f \tag{12}$$

$$\sigma_c = \frac{M_x z E_c}{D}, \qquad |z| < \frac{t_c}{2} \tag{13}$$

The stresses still vary linearly in the z direction but there is a jump at $z = t_c/2$ due to the difference between E_f and E_c.

The direct stresses from the in plane load N_x, cf. Figure 3, also differ between the faces and core due to the fact that the direct strain is equal across the cross section. The strain from N_x, for a sandwich beam with similar faces, is given by

$$\varepsilon_{Nx} = \frac{N_x}{2E_f t_f + E_c t_c} \qquad (14)$$

Here N_x is force per unit of length (y-dir in Figure 3). Face and core direct stress is than simply calculated by multiplying with the corresponding modulus of elasticity. Once again one realises that the direct stresses in the faces will be much larger than those in the core (exactly E_f/E_c times larger) and even thou the face material typically is much stronger than the core, the yield or fracture strain will likely be lower. This will be discussed further in chap. 5.5.

Once the strains and stresses due to bending and in-plane loads are calculated they may be superimposed to evaluate the effective stress in the beam [2].

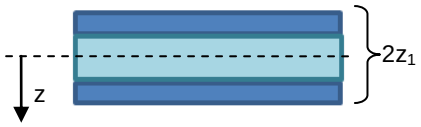

Figure 6, sandwich beam

A common expression for the shear stress of a beam in bending, *thickness* = $2z_1$, can be derived from the equilibrium equations of a sub-area, and is given by [2]

$$\tau_{xz}(z) = \int_z^{z_1} \frac{d\sigma_x}{dx} dz\,, \qquad |z| < z_1 \qquad (15)$$

since $\tau_{xz}(z_1) = 0$, see Figure 6.

Inserting the stress from eq. (12) into the above equation and applying the geometry in Figure 1 and Figure 3 one receives

$$\tau_{xz}(z) = \int_z^{\frac{d+t_f}{2}} \frac{d\sigma_x}{dx} dz \rightarrow \quad \text{eq.(12)} \quad \rightarrow \int_z^{\frac{d+t_f}{2}} \frac{d\left(\frac{M_x z E}{D}\right)}{dx} dz = \frac{dM_x}{dx} \int_z^{\frac{d+t_f}{2}} \frac{zE}{D} dz, \quad T_x = \frac{dM_x}{dx} \rightarrow$$

$$\tau_{xz}(z) = \frac{T_x}{D} \int_z^{\frac{d+t_f}{2}} E z dz \qquad (16)$$

This results in two equations for the shear stress

$$\tau_c(z) = \frac{T_x}{D} \int_z^{\frac{d+t_f}{2}} E z dz = \frac{T_x}{D} \int_{\frac{d-t_f}{2}}^{\frac{d+t_f}{2}} E_f z dz + \frac{T_x}{D} \int_z^{t_c/2} E_c z dz\,, \qquad |z| < \frac{t_c}{2} \qquad (17)$$

$$\tau_f(z) = \frac{T_x}{D}\int_z^{\frac{d+t_f}{2}} E_f z dz\,, \qquad \frac{t_c}{2} < |z| < \frac{t_c}{2} + t_f \tag{18}$$

Calculated, eq. (17) and (18) assume the following two expressions

$$\tau_c(z) = \frac{T_x}{D}\left[\frac{E_f t_f d}{2} + \frac{E_c}{2}\left(\frac{t_c^2}{4} - z^2\right)\right], \qquad |z| < \frac{t_c}{2} \tag{19}$$

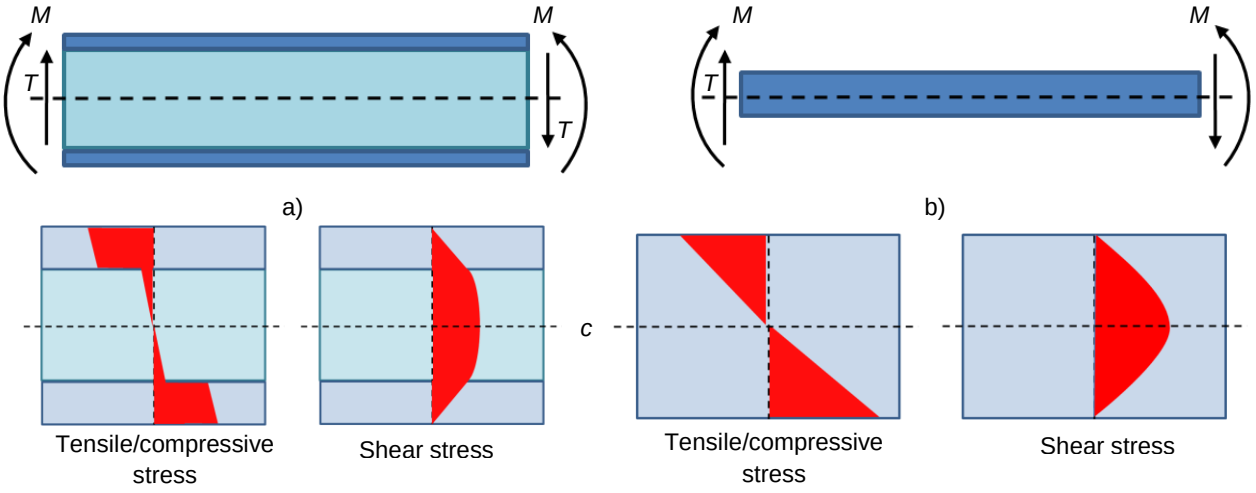

Figure 7, stress distributions in a sandwich beam (a) and a solid beam (b) when bending moment *M* and transverse force *T* is applied. *c* = centroidal line of beam

$$\tau_f(z) = \frac{T_x}{D}\frac{E_f}{2}\left[\left(\frac{t_c}{2} + t_f\right)^2 - z^2\right], \qquad \frac{t_c}{2} < |z| < \frac{t_c}{2} + t_f \tag{20}$$

The stresses in equation eq. (12) and (13) as well as the shear stresses in eq. (19) and (20) are illustrated in Figure 7 for both a solid beam and a sandwich beam. As shown in the figure, the faces in the sandwich beam withstand most of the compressive and tensile stresses whilst the majority of the shear stress is situated in the core.

Given the correct circumstances there are several approximations that can be made to the stiffness and stresses in the sandwich structure [2]. From Figure 5 it is clear that the main stiffness is from the term D_0. By dividing $2D_f$ and D_c with D_0 in eq. (11) the following expressions are attained

$$\frac{2D_f}{D_0} = \frac{1}{3}\left(\frac{t_f}{d}\right)^2 < 0.01 \leftrightarrow \frac{t_f}{d} < 0.173 \tag{21}$$

$$\frac{D_c}{D_0} = \frac{1}{6}\frac{E_c {t_c}^3}{E_f t_f d^2} < 0.01 \qquad (22)$$

Equation (21) is pretty straight forward and states that if *d* is about 5.8 times greater than t_f the term $2D_f$ is less than 1% of D_0. The relationship in eq. (22) is not as simple and depends both on the relationship between t_f and t_c as well as E_f and *Ec*. If however $E_c << E_f$ it is often safe to assume that the term D_c will have negligible influence over *D*. Now if both $t_f << t_c$ and $E_c << E_f$ than $D \approx D_0$. Commonly, when engineering sandwich structures, the core to face thickness ratio is in the order 10 to 50, and the face to core Young modulus ratio is in between 50 and 1000 [2].

In the same sense the stress distributions can be approximated to assume constant stresses throughout the core and faces [2]. If we assume $D \approx D_0$, i.e. $E_c << E_f$ and $t_f << t_c$, eq. (12), (13), (19) and (20) may be approximated to

$$\sigma_f = \pm\frac{M_x}{t_f d} \qquad (23)$$

$$\sigma_c = 0 \qquad (24)$$

$$\tau_f = 0 \qquad (25)$$

$$\tau_c = \frac{T_x}{d} \qquad (26)$$

A graficall representation of these stresses is given in Figure 8.

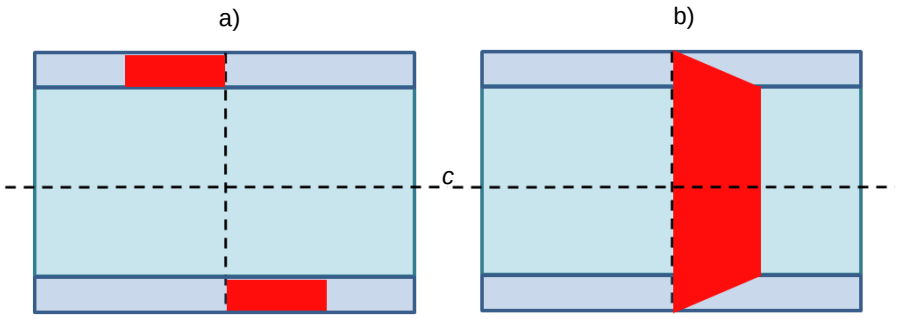

Figure 8, approximation of stress distributions in a sandwich structure.
a) direct stress
b) shear stress
c = centroidal line

2.1 Pros and cons of sandwich construction

As implied earlier one of the major benefits with sandwich structures is the reduced weight to strength- and rigidity ratio. Compared to classical stiffened faces, e.g. truss stiffeners, the sandwich structure offers continuous stiffness. When using composites for the skin elements the strength to weight ratio is even greater than that of metal sheet. Composites also offer flexible design when considering complex profiles.

The characteristics of a sandwich structure offer a wide range of optimization alternatives. The structure can be optimized for thermal insulation, acoustic damping [19], energy absorption from impact [18], weight minimization [19], stress, strain and stiffness optimization [7], [17], [19] or other structural characteristic that may be of interest.

According to the Technology Information, Forecasting and Assessment Council (TIFAC), the main advantages of sandwich construction are:

- High rigidity combined with higher strength to weight ratio
- Smoother exterior
- Better stability
- High load carrying capacity
- Increased fatigue life
- Crack growth and fracture toughness characteristics are better compared to solid laminates
- Thermal and acoustical insulation
- High bi-axial compression load bearing ability

On the other hand several new challenges arise with sandwich construction. Because of the limited knowledge and routine of sandwich design in the industry, knowledge that has been built up for many decades regarding conventional materials, introducing sandwich construction also introduces several unknown factors, e.g. fire safety, recyclability and ageing effects. Some sandwich construction may involve large capital investments in the form of new equipment and several of the materials used for sandwich structures are more expensive than conventional materials. These factors are especially true for composites laminates which, furthermore, together with foam cores, have lower temperature tolerances than conventional metals. Sandwich panels may also fail in different ways in comparison to classic panels and the relatively weak core makes the sandwich structure sensitive to concentrated loads around for example fastenings.

Whether or not sandwich design is the right way to go is a complex question. However, with respect to weight saving, it is not farfetched to assume that there is no other engineering material that can outperform sandwich structures.

3 Sandwich solutions

There is an almost endless amount of combinations of materials that can be used in sandwich construction. For optimal stiffness metal sheet may be appropriate for the face material, however, composites can often offer a better strength to weight ratio. Cores for load carrying sandwich structures also come in a vast variety but can in general be divided into four main groups; foam cores, honeycomb cores, concrete cores and balsa cores.

3.1 Cores

There are several different material types to choose from when constructing a sandwich with a foam core, e.g. polyurethane foam (PUR), polystyrene foam (PS), polyvinyl chloride foam (PVC), polymethacrylimide foam (PMI), etc. Among these PUR and PS foams are most commonly found as insulation or other non-load bearing applications, whilst PVC and PMI foams offer a higher strength to density ratio [2]. Also honeycomb cores come in a variety of materials, e.g. aluminium, aramid, fibre-glass, etc.

The most important characteristics of the core are: low weight, shear modulus, shear strength and stiffness perpendicular to the faces.

Below a comparison of the structural properties for different core alternatives from some mayor manufactures can be found [20], [21], [22], [23], [24], [25], these values correspond well to typical mechanical properties for the materials in question [2]. Unfortunately, DOW, cf. [25], had limited information about their higher density extruded polystyrene foams, i.e. “Highload” 40, 60 and 100 (the numbers stand for compressive strength in psi). For other manufactures see for example [13].

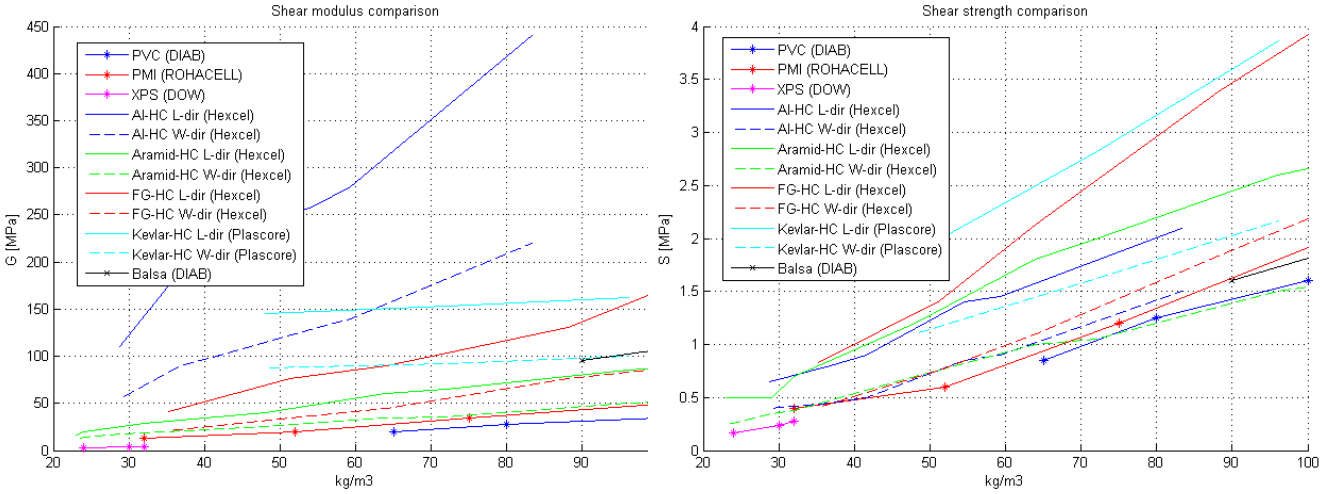

Figure 9, Comparison of shear properties, left: shear modulus, right: shear strength.
HC = honeycomb, Al = aluminium, FG = fibreglass, XPS = extruded polystyrene
Plascore’s values from Higher Shear configuration honeycomb

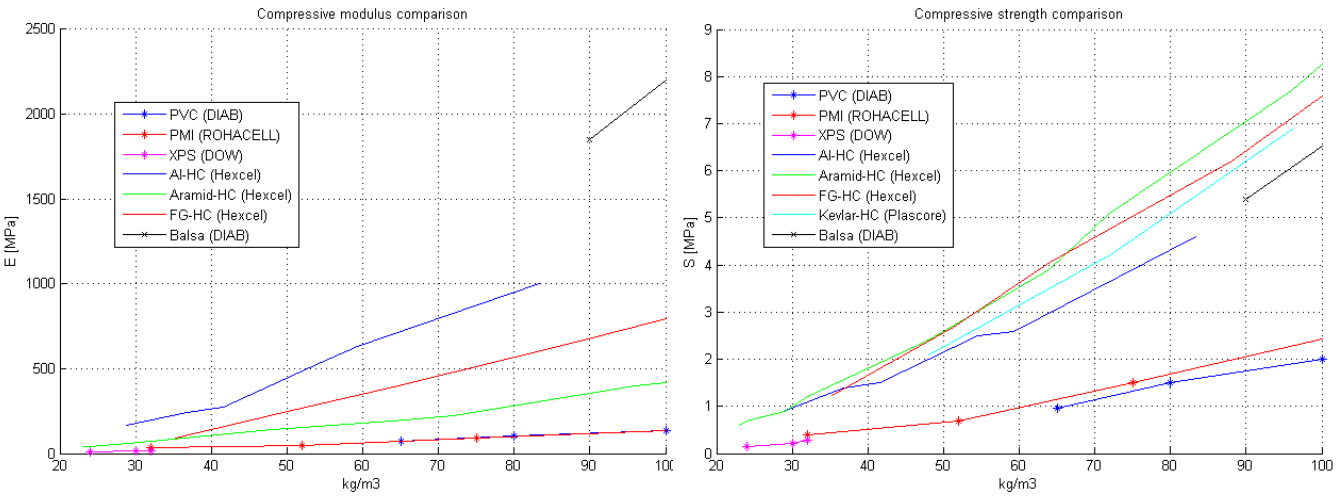

Figure 10, Comparison of out of plane compressive properties, left: compressive modulus, right: compressive strength (HC = honeycomb, Al = aluminium, FG = fibreglass, XPS = extruded polystyrene)
***OBS**: Compressive modulus for Rohacell PMI not actually a compressive modulus but according to Röhm a Modulus of elasticity evaluated from a tensile type test*
Compressive modulus for DOW XPS not actually compressive modulus but a flexural modulus
Compressive modulus not found for Plascore Kevlar honeycomb

From Figure 9 and Figure 10 it is apparent that core properties can be approximated to functions of core density, e.g.

$$E_c = C_E \rho_c^n \quad (27)$$

$$G_c = C_G \rho_c^n \quad (28)$$

The constants C_E, C_G and n can be estimated from, for example, the curves presented in Figure 9 and Figure 10. Curves covering a greater mass-span are presented in the Appendix. One interesting observation that can be made in Figure 9 is that the honeycomb cores shear modulus, in particular that of the Kevlar honeycomb, does not seem to converge towards *0* for decreasing densities in the same manner as the foam cores. n in eq. (28) can possibly be approximated to *2* for the foam cores, while the Kevlar core data indicates a $n < 1$.

Honeycomb cores have varying properties in different direction because of the manufacturing process which results in double cell-walls in one direction and single in the other [2]. This is illustrated in Figure 11 as well as the directions *W* and *L*. The "jumpy" behaviour of the honeycomb-cores in Figure 9 and Figure 10 is most likely due to varying cell sizes. Still the figures give a good assessment of the core properties.

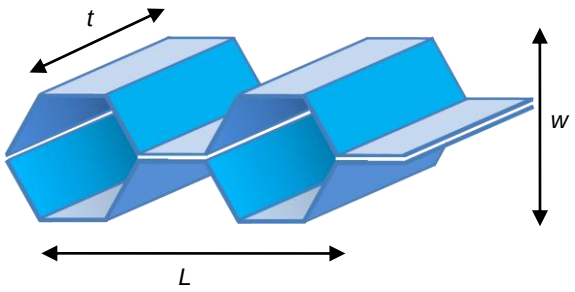

Figure 11, honeycomb dimensions

One can further imagine a honeycomb sandwich panel consisting of cells themselves constructed by sandwich structure, a foam filled honeycomb core, a corrugated core with sandwich structure for reinforcement and this leads to a foam filled corrugated core, etc. Once again there is an endless amount of options which only are restricted by the imagination. From a realistic stand point the restrictions arise from manufacturing costs. Of these “special” core solutions the foam filled honeycomb core seems to be the most common solution available from suppliers.

Other important properties that should be taken into consideration are thermal conductivity, acoustic damping, water resistance, fire resistance and ageing effects.

3.2 Faces

Compared to the core important face properties are high tensile and compressive strength and elasticity modulus. For sheet metals this is quite straight forward, isotropic materials with well defined values. Composite skins on the other hand have varying properties in different directions because of their anisotropic nature, but on the plus side commonly have higher strength to weight ratios.

Common sheet metals are, e.g. steel, aluminium and titanium. For composite faces one could consider carbon fibre-, glass fibre- or aramid-laminates. Composite skins, or laminates, consist of a number of lamina. A lamina is a thin orthotropic, or anisotropic, layer of either unidirectional, in some way woven, or random reinforcement fibres and a matrix material. The matrix’s purpose is to bind the fibres together in their specified position and orientation and transfer loads to the reinforcement. There are three groups of matrix materials, i.e. organic, metallic and ceramic. Of these organic, and especially epoxy resins, are by far the most common structural resin for high-end applications [26].

Highest strength is achieved from unidirectional fibre mats. However, these laminas only display high strength in on direction, i.e. the fibre direction, and low to very low perpendicular to this direction. For optimum load bearing capacity and minimum crimp, in more than one direction, several unidirectional layers can be “stitched” together instead of somehow weaving the reinforcements. This way the reinforcement in each direction is kept plane. The “stitched” fabric has similar properties of a multi layered unidirectional laminate, i.e. a laminate made up of several unidirectional laminas with varying global fibre orientations. The difference is that the “stitched” fabrics are easier to handle prior to curing.

The addition of resin to the laminate affects the mechanical properties of the skins which will be a combination of the properties of the reinforcement as well as the resin material. D Zenkert has summarized how to estimate these properties in [2 chap. 2.2]. The estimations are derived by weighing the mechanical properties of the reinforcement and resin to their weight ratios in the laminate.

To get some idea of the different characteristics of composite laminates compared to metal sheets Figure 12 gives a comparison of tensile strength and modulus for some epoxy prepreg laminates from Hexcel [23].

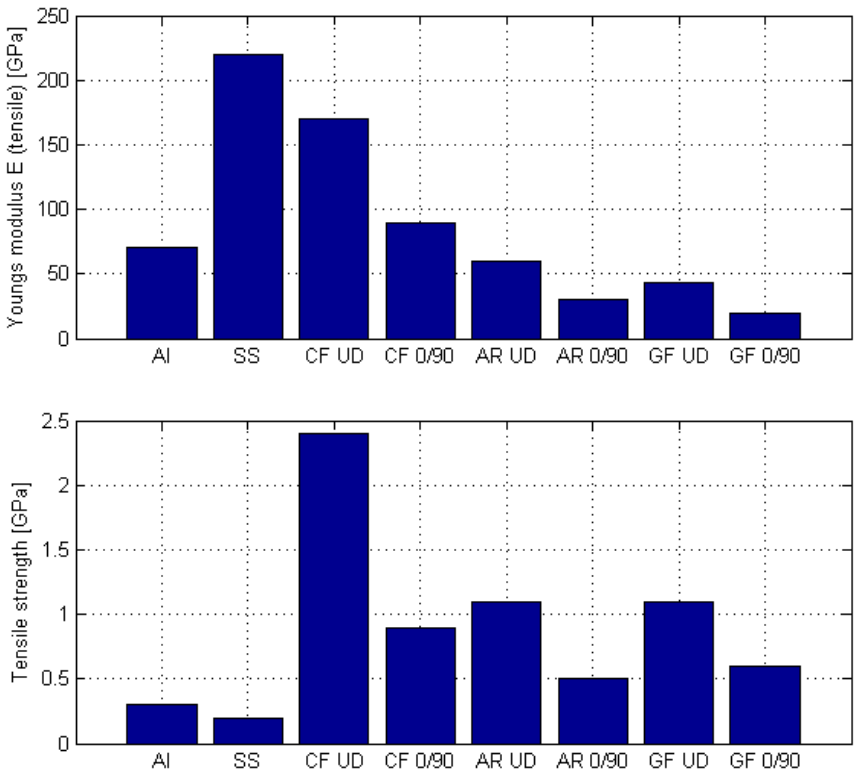

Al: Aluminium
SS: Stainless steel
CF: Carbon fibre
AR: Aramid fibre
GF: Glass fibre
UD: Unidirectional
0/90: Bi-directional

Strength and modulus in fibre direction of unidirectional specimens (0°)

Figure 12, comparison of tensile strength and modulus of two metals and some epoxy prepreg laminates. Values vary significantly between different types of specific materials, values above are only examples.
Fibre volume content of carbon ≈ 60% [23]
Fibre volume content of glass/aramid ≈ 50% [23]

The strength and modulus in the transverse in-plane direction for the unidirectional laminates are roughly 97% and 80 - 95% lower respectively in comparison to the corresponding values presented in Figure 12, while the bi-directional laminates show very little to no difference in the two directions. It should also be mentioned that the density of the composites laminates range from around 1000kg/m^3 to about 2000kg/m^3, whilst steel and aluminium have densities of about 7900kg/m^3 and 2700kg/m^3 respectively.

To sum up, the mechanical properties of a composite laminate are dependent on the reinforcement material, fibre properties, fibre direction in each lamina, choice of weave style, number of lamina in the laminate, grouping order of the lamina, resin properties and volume/weight ratio between reinforcement and resin. This results in that a composite laminate may have differing strength and modulus not only for compressive, tensile and flexure tests but also varying strength and modulus in each direction. Even though this may complicate the choice of face make-up for sandwich structures, the characteristics of composite laminates enables the engineer to utilise the materials full potential in different applications by tailoring directional stiffness and strength properties.

Other properties that should be taken under consideration are for example impact resistance and environmental resistance.

3.3 Manufacturing sandwich structures

As well as considering the structural properties of the finished sandwich structure one should also consider the manufacturing process when looking at sandwich construction as this differs between solutions. As an example certain manufacturing processes eliminate the need of a bonding layer between the faces and core, usually saving both time and money. However, choice of manufacturing process is not always an option but limited by choice of sandwich design.

The different manufacturing processes range from manual Wet-layup, i.e. hand-layup of composites, to fully automated continuous production [8]. Depending on the production size, essential performance qualities and time schedule one may consider several possibilities.

Layup processes are common when considering composite face panels. Most of these require a large amount of manual labour. The basic idea is to use a one- or two-sided mould of the sandwich panel and in this mould combine the resin and reinforcement materials for the face. This can either be done directly on the core, where the core than acts as the mould, or the core and face can be combined in a later stage by adhesive bonding.

Prepregs, i.e. pre-impregnated reinforcement fibres or fabrics, can also be placed in a mould or directly onto the core. Prepregs usually offer higher-performance materials compared to the ones used in other layup processes [8]. This method requires applied heat for the cross linking of the resin material since the resins in the prepregs should not cure during layup at room temperature. Prepreg layup can be fully automated, and there are numerous different process methods [11].

When face elements and core are produced separately, for example when using metal sheet faces, or honeycomb core, the different components are bonded with an adhesive. The adhesive is placed between the face and core and the structure is subjected to the required pressure and/or temperature of the adhesive resin. For high performance structures the bonding procedure may require a vacuum and/or an auto-clave.

Another common manufacturing process is liquid moulding. There are several different methods for liquid moulding, e.g. resin transfer moulding, structural reaction injection moulding or vacuum injection moulding. The general idea is to use a closed mould containing both reinforcement and core material. The resin is then injected by use of vacuum or pressure. The curing process, if needed, can then be achieved by either heating the mould or its' surroundings.

Schindler Wagon developed a unique technique for constructing a rail carriage; a large filament winding machine able to wind an entire carriage in eight days [10]. The fibres or filament, are impregnated with unsaturated polyester resin and wound around a mould of the carriage, building the carriage from the inside out. When a sufficient layer has been wound a foam core is placed on the inner wound and the outer skin is then wound on top.

There are methods that more or less produce continuous sandwich panels [8] which is of course favourable from an economical stand point. These methods often restrict the complexity of the panels, i.e. constant thickness, no complex profile, etc.

The manufacturing process can have significant impact on mechanical behaviour of the sandwich structure. For instants G. Belingardi et al. noticed that the Young modulus decreased linearly with respect to the thickness of the laminates [18]. The shifting thickness of the laminates was caused by a varying amount of resin used during manufacturing whereas the fibre quantity was constant. This results in a shifting resin to reinforcement ratio between laminates which in turn resulted in data scattering during tests.

4 Sandwich technology in transportation vehicles

Sandwich structures are not only found in manmade constructions but also in nature where the combination of high strength and low weight is of utter importance. For example the bones in human and animal skeletons are comprised of sandwich structures with foam-like cores as well as the branches of some trees and plants.

During the Second World War England made use of a plywood sandwich structure in the Mosquito night bomber. During the same time the USA looked at sandwich structures with faces of reinforced plastics. In 1943 the Wright Patterson Air force Base used fibre-glass reinforced polyester as skin material together with both a balsa and honeycomb core [1].

Sandwich is especially popular in aerospace and marine applications, e.g. passenger planes, space shuttles, satellites, pleasure boats and navy applications. Almost half of the wetted surface area of the Boeing 757/767 is honeycomb sandwich [1], and the first non-government funded space ship had, among other things, wings constructed in sandwich with carbon fibre reinforced polymer epoxy skins and honeycomb core. During the 70s Karl-Axel Olsson led the development of sandwich technology in Scandinavia by convincing several of the nation's naval forces to change from steel to fibreglass sandwich hulls.

In ground transportation sandwich structures can be found in cars, busses and trains. Since the 80s front cabs of locomotives have been built with sandwich technology because of its high strength and good impact and energy absorption properties. Some examples of this are the XPT locomotives in Australia, the ETR 500 locomotives in Italy, the French TGV and the Swiss locomotive 2000 [1]. Two other large projects within rail are Bombardier Transportation's C20 FICA and the Korean Tilting Train Express. In these projects sandwich construction was utilized for the entire car body, therefore, these are examined closer in Chapters 4.1 and 4.2. Furthermore a light weight low floor bus concept is presented in 4.3.

4.1 C20 FICA

The C20 FICA has been in operation in the Stockholm metro system since July 16 2003. FICA is a “Flat package” concept, i.e. the car body is made up of several modules that are bolted together. Compared to the conventional C20 the FICA system has introduced large scale lightweight sandwich panels into the load bearing construction. This has increased the aisle space with 30% and reduced the tare weight per passenger by about 8%.

The C20 FICA is a 3-car unit, cf. Figure 13, with a total length of 46.5m and an operating speed of 80-90km/h.

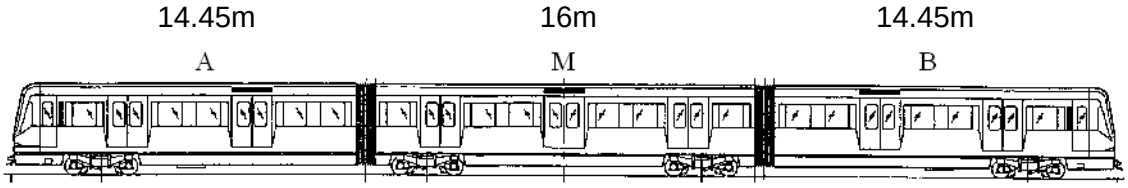

Figure 13, vehicle configuration of C20 FICA [33].

4.1.1 Sandwich structure

The C20 FICA body structure consists of sandwich panels in the sides, roof and floor. End beams where inserted into the sides as supports, see Figure 14. Material properties can be found in Table 2 [33].

#	Unit	Material	Thickness [mm]
1	Face	Stainless steel	0.6/0.8*
2	Core	PMI foam	30-50
3	End beam	Stainless steel	1.25-3
4	Overlap length	-	50-80**
5	Adhesive	Epoxy	0.3-1

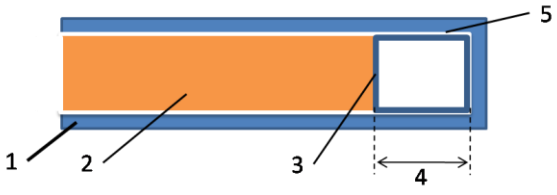

Figure 14, Sandwich structure of C20 FICA
**inner/outer face*
***Not thickness as illustrated in figure*

Property	Stainless steel	PMI foam
Density ρ, [kg/m^3]	7820	41.5, 110, 160
Young’s modulus E, [GPa]	196	0.032, 0.150, 0.236
Shear modulus G, [GPa]	76	0.014, 0.055, 0.085
Poisson’s ratio v, [-]	0.29	0.167, 0.364, 0.387
Yield stress, [MPa]	210, 350, 550	-
Ultimate stress, [MPa]	520, 550, 830	-

Table 2, material properties for the constituents of the FICA sandwich structure.
Different grades of steel and foam where used as shown in the table

Another essential element is the adhesive bond between the core and skin. This constituent will not be examined closer in this study. However, some important characteristics of the adhesive joint in sandwich construction in general are mentioned in Chap. 5.

4.1.2 Car body dynamics

Eigen frequencies from FE calculations and tests on the FICA units can be found in Table 3 and Table 4 respectively. The calculated Eigen frequencies are for the fully equipped car whilst the measurements where performed with only structural parts, inner floor and insulation mounted.

Mode	A/B-car	M-car
1st vertical bending mode	10.4 Hz	9.65 Hz
1st rhombic mode	9.18 Hz	8.18 Hz
1st torsion mode	10.4 Hz	9.78 Hz
1st lateral bending mode	>20 Hz	14.7 Hz

Table 3, Eigen frequencies derived from FE-analysis of the C20 FICA [33]

Mode no.	Frequency [Hz]	Damping, (viscous) [%]	Description
1	14.8	0.8	1st torsion mode
2	15.3	1.2	1st vertical bending mode
3	16.8	1.1	1st rhombic mode
4	23.6	0.1	Complex mode shape

Table 4, Eigen frequencies derived from measurements on the C20 FICA B-end coach [30].

As shown above the calculations differ from the tests in two ways, first off the order of the modes do not match, secondly the measured frequencies are significantly higher than their calculated equivalents. This can partially be explained by the differing loads in the vehicles as well as modelling problems and uncertainties in the modelling of sandwich structures and adhesive parts. An updated FE-model was also constructed to more accurately represent the measurement conditions. Even though the results from these calculations agree better with the measured results, the difference is still significant, cf. Table 5

Mode	Updated FE-model [Hz]	% higher frequency during test compared with calculations
1st vertical bending mode	11.6	32
1st rhombic mode	11.0	53
1st torsion mode	12.9	15

Table 5, difference in Eigen frequencies between calculations and tests (B-car) [30].

The C20 FICA structure has given, as mentioned, increased interior space, thus increasing passenger comfort and mobility. The reduced weight enables increased passenger loading capacity or lower energy consumption and lower maintenance cost. The sandwich design has also reduced assembly effort and development time because fewer parts are needed to cover all the integrated functions of the sandwich panel, e.g. sound reduction, insulation etc. The system however encountered several problems*:

- No set fire standards.
    - This results in that agreements need to be set for each costumer.
- The sandwich system was not optimal for the floor.
    - The floor required additional mineral wool for the fire barrier which eliminated eventual weight and space savings in the floor.
- Manufacturing had to be strictly controlled.
- Less tolerant to major external damage.
    - Repair and adjustment was as complicated as for the conventional vehicle.
- Poor agreement was recognized between calculations and tests.
    - As shown in chap. 4.1.2.

**Problem source: L Nilsson "Bombardier FICAS* Overview", 2004-02-25.*

4.2 Korean Tilting Train eXpress, TTX

The train lines in Korea have many curves due to the high amount of mountains covering the land area. This limits the speed-up of conventional trains and additional maintenance is needed for high speed trains to operate on the conventional lines. To reduce the risk of overturning in curves at high-speed and passenger discomfort from high centrifugal forces the Tilting Train eXpress has been developed [4]. To reduce the wear and tear on the tracks the TTX upper body was constructed of a lightweight sandwich structure with a supporting inner frame around windows, doors and other openings. The under frame is manufactured of conventional stainless steel introducing a low centre of gravity thereby increasing stability during curves. The steel under frame also provides increased stiffness against global bending.

A preliminary design of the car body was without the supporting inner frame. However, during verification calculations, the deformation of the body shell during vertical loading was deemed excessive. In order to reinforce the structure the inner frames were inserted into the sides, roof and end structures of the car body [4].

The TTX was designed to run at 200km/h and is composed of 4 motorised cars and two trailers as shown in Figure 15.

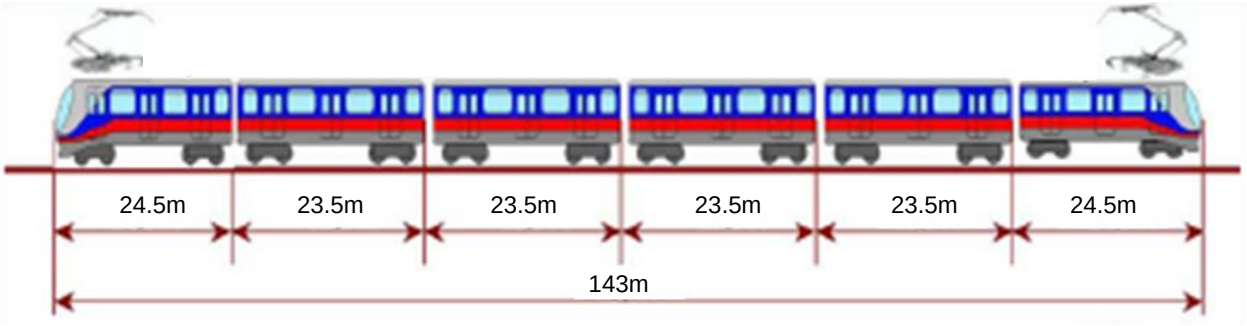

Figure 15, vehicle configuration of TTX [16].

The sandwich structure elements consist of carbon fabric/epoxy prepregs for the faces and an aluminium honeycomb core. The entire car body is manufactured as one single structure. This was accomplished by means of large scale auto-clave. A large mould was built in which the outer face was firstly laid out. The outer face was than cured in the auto-clave. Secondly the inner frame and honeycomb core was placed on top of the outer skin. The core and skin was bonded by use of an adhesive film. After this step followed lay-up of the inner face. Lastly the entire structure was, after appropriate vacuum bagging, cured in the auto-clave. By constructing the entire car body as one structure weak links between panels are eliminated. The only remaining weak link is between the upper body and under frame [6].

The sandwich structure reduced the upper car body weight by 39% compared to a stainless steel car body. The total weight reduction, including under frame, was 28% [4].

4.2.1 Sandwich structure

The TTX sandwich structure consists of an outer and inner face of graphite/epoxy resin and an inner core of aluminium honeycomb as shown in Figure 16.

#	Unit	Material	Thickness [mm]
1	Face	Graphite/epoxy prepreg	1.5/3.5*
2	Core	Aluminium honeycomb	37
3	Inner frame	Steel	2
4, 5	Overlap length	-	50, 40**
6	Adhesive	-	-

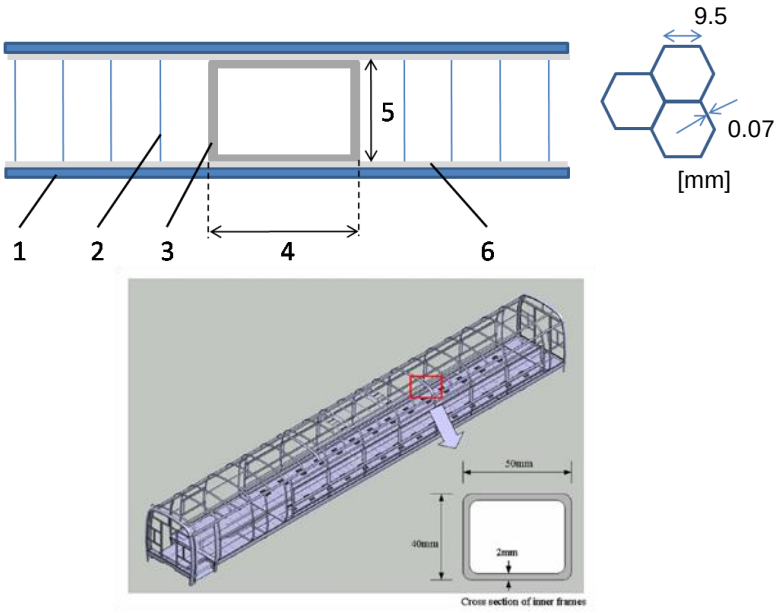

Figure 16, sandwich structure and inner frame of the TTX car [4], [12].
**Inner/outer face*
**Not thickness as illustrated in figure*

Core – Aluminium honeycomb	
Property	**Value**
E_1 [GPa]	0.17
E_2 [GPa]	0.17
G_{12} [GPa]	1480
S_1 [MPa]	150
S_2 [MPa]	250
S_{12} [MPa]	170
v [-]	0.996
ρ [kg/m^3]	55

Table 6, core properties of the TTX sandwich structure, *S* = strength [6].

Face – Graphite/Epoxy Fabric	
Property	**Value**
E_{t1} [GPa]	55.5
E_{t2} [GPa]	48.3
E_{c1} [GPa]	52.6
E_{c2} [GPa]	52.1
G_{12} [GPa]	3.81
S_{t1} [MPa]	936
S_{t2} [MPa]	885
S_{c1} [MPa]	542
S_{c2} [MPa]	513
S_{12} [MPa]	103
v [-]	0.099

Table 7, face properties of the TTX sandwich structure, *t = tensile, c = compressive, 1 = warp direction, 2 = fill direction, S = strength* [14].

Under frame - Steel	
Property	**Value**
ρ [kg/m^3]	7900
E [GPa]	183, 200, 210
V [-]	0.3
S [MPa]	220, 250, 370

Table 8, under frame properties of the TTX sandwich structure, three different types of steel where used *S* = strength [6]

Material properties for the different constituents of the TTX sandwich structure can be found in Table 6, Table 7 and Table 8 [6]. It is not clear from [6] which directions the subscripts 1, 2 and 12 represent for the honeycomb core in Table 6. In accordance with previous discussion the core properties can be approximated to functions of core density and with help from the curves presented in chap. 3.1, an aluminium honeycomb core of density 55kg/m^3, would have a compressive out of plane strength of about 2.5MPa, a compressive modulus of 540MPa, shear strength of 1.4/0.85MPa (*L*-dir/*W*-dir) and a shear modulus of 260/130MPa (*L*-dir/*W*-dir). Most of these values do not agree with the values presented in Table 6. The compressive modulus is, however, in the same order of magnitude as E_1 and E_2, while the strengths are about 100 times larger and the shear modulus, G_{12}, is about 10.000 times larger. Interestingly, in [6], it seems as

if the only properties of the core that were not supplied by the manufacturer were the stiffness modulus E_1 and E_2 which were derived by calculations based on the geometric shape of honeycomb. It is uncertain what the reasons for the extraordinary values are but they could be simple decimal and/or unit errors. No further effort is put into finding an explanation at the moment.

Furthermore, no consideration is given for varying properties in shear in the *W*- and *L*-directions of the honeycomb (cf. Figure 11). The density of the core is also quite high with respect to the given geometry and should be closer to 30kg/m^3. This may be explained by some sort of protective coating used on the core, thus increasing the actual weight.

The face properties are given for the in-plane directions of the warp and fill, cf. Table 7. When weaving the *warp* is the in-plane longitudinal direction and *fill* is the in-plane transverse direction. In this case the values show good concurrence with the bidirectional carbon fibre prepreg presented in chap. 3.2.

4.2.2 Car body dynamics

Several analyses and measurements on structural strength, deflections under loading and other mechanical characteristics have been carried out on the TTX; [4], [6], [12], [14], [15], [16], [17]. The car body had the following design criteria: no Eigen modes under 10 Hz, withstand end compressive test of 1200kN, vertical load test of about 360kN (differs between papers), maximum deflection under vertical load of <1/1000 of the distance between bogie centres (<15.9mm) and exhibit an equivalent bending stiffness, cf. eq. (29), greater than 6x10^{14}Nmm^2.

$$EI_{eq} = \frac{w_0 L_2^2}{384\delta}(5L_2^2 - 24L_1^2) \qquad (29)$$

W_0: vertical load per unit length, L_1: distance between car end and bolster centre, L_2: is distance between bolster centres, δ: maximum deflection of the car body.

The car body was also subjected to torsional, twisting tests and 3-point support tests (lifting test) in accordance with the Japanese rolling stock standard JIS E 7105.

The FE analysis in [6] and [12] showed Eigen modes of 11.67 Hz in vertical bending and 14.39 Hz in twisting. The measured Eigen modes in [12] where, however, 10.25Hz and 11.0Hz in bending and twisting respectively. These modes are within design limits but show a 12% and 24% deviation from FE analysis, cf. Table 9.

Mode	FEA	Test	% lower frequency during test compared with calculations
1st vertical bending mode	11.67 Hz	10.25 Hz	12
1st twisting mode (torsion)	14.39 Hz	11.0 Hz	24

Table 9, Eigen frequencies derived from FE-analysis and test on the TTX

The maximum stresses in the upper car body during load simulations were found around the window and door openings and scaled about 60MPa, well below the strength of the graphite/epoxy. The car body's equivalent bending stiffness was first measured to

$8.1x10^{14}Nmm^2$, which was calculated from a deflection of 12.3mm under vertical loading of 363kN [12], [14]. In [15], on the other hand, a stiffness of $7.5x10^{14}Nmm^2$ is calculated from a deflection of 9.25mm (as this makes no sense a closer look revealed that different loads where used, the later using 252.5kN). Even though these results only differ by about 8%, this brings to light if the equivalent bending stiffness formula used in eq. (29) is accurate or if measuring procedures have been inaccurate.

4.3 Korean low floor bus

The Korean low floor bus (KLFB) has been developed to ease access in and out of the vehicle and has a floor height of 25-34cm above road level [39]. It is also said to be the first intercity bus to be subjected to weight limitations under the financial support of the Korean Ministry of Construction and Transportation [38].

In [38] a couple of sandwich panel candidates where studied for use in the KLFB. Since this is the only research document found on this subject the panels are presented here as the ones used for the car body, however, as mentioned, these are only candidates and not confirmed to be the actual panels in the KLFB.

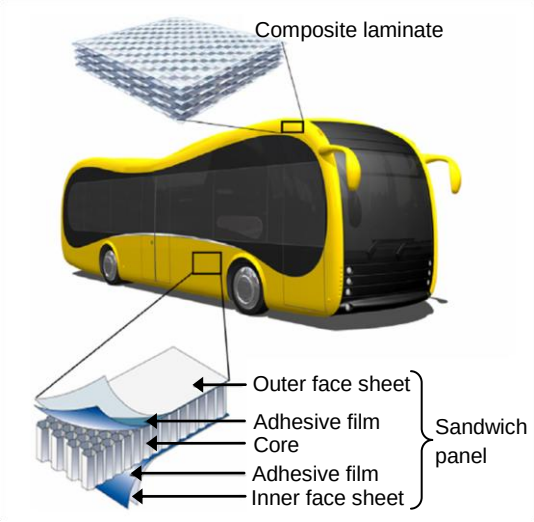

Figure 17, KLFB body and panel design [38].

In [38] the panels are divided into two groups, one for the floor structure and the second for the walls and roof. The first is comprised of an aluminium face sheet with an aluminium honeycomb core or a foamed aluminium core (the foamed aluminium seems to be a closed cell foam with regard to pictures presented in [38]), whilst the second is made of a glass fabric-epoxy prepreg face sheet with a balsa or aluminium honeycomb core [38]. Also, laminated composites are used for more complex geometries where sandwich design is said to be too difficult. Figure 17 depicts the car, sandwich panel and composite laminate design of the KLFB. The sandwich panels for the walls and roof are designed with unequal face sheet thickness for the inner and outer faces, 1.5mm and 3mm respectively, whilst the floor has the same thickness for the inner and outer face, 1.2mm. The core dimension also varies between the two sandwich groups. The core thickness for the sides and roof structures is 25.4mm while the sandwich panels in the floor have a core thickness of 16.0mm. Face and core material properties can be found in Table 10 and Table 11 respectively.

Face sheet	**Direction**	**Tensile**		**In-plane shear**		**Density [kg/m^3]**
		Modulus [GPa]	*Strength [MPa]*	*Modulus [GPa]*	*Strength [MPa]*	
Glass fibre	*Fill*	20.81	424.83	4.20	85.77	1850
	Warp	18.71	414.88			
Aluminium	-	70.30	193.00	25.90	138.00	2680

Table 10, face sheet properties of the KLFB sandwich structure [38].

Core	Compressive		Shear		Density [kg/m^3]
	Modulus [GPa]	*Strength [MPa]*	*Modulus [GPa]*	*Strength [MPa]*	
Aluminium honeycomb	1.37	2.55	0.51	1.72	59
Balsa	3.92	12.67	0.16	2.94	151
Foamed aluminium	4.67	3.17	1.73	9.20	473

Table 11, core properties of the KLFB sandwich structure [38].

Apart from for the aluminium honeycomb modulus in compression and shear, which are twice as large, the values for the aluminium honeycomb and balsa core correspond perfectly with the curves presented in Figure 9 and Figure 10. Furthermore, as for the TTX evaluation, no consideration has been taken for varying shear properties in the *L* and *W*-directions of the honeycomb core, cf. Figure 11.

All sandwich panels utilised the same adhesive for bonding between face sheets and core, additionally this was the same adhesive used for the TTX; Bondex® 606, a high temperature epoxy adhesive film. As for the TTX, the KLFB face sheets and core where bonded and cured in an autoclave.

In [38], Kwang Bok Shin et al., evaluate the impact response of the sandwich panels presented above where they conclude that glass fabric epoxy sandwich panels, in comparison to the aluminium sheet skins, are excellent candidates for the primary structural material of the transit bus. Furthermore the glass fabric skins with honeycomb core showed the best performance as well as the lowest weight.

The KLFB seems to be an almost brand new project, having trial rides as late as June of this year (2009) [39].

4.4 Other existing research

A.M. Harte et al. performed a multi-level approach on weight optimisation for a “typical” rail vehicle body shell [7]. The sandwich structure properties are given in Table 12 and Table 13. Initially the sandwich panel configuration was a 28mm thick polyurethane core with two 8mm thick face sheets of glass fibre reinforced epoxy composite plies giving a total of 16 plies and a lay-up of $[0°/\pm45°/90°]_{S2}$. Each ply was 1mm thick. This gave a total panel thickness of 44mm. The panels where supported by a frame of steel stiffeners. The car body was furthermore subjected to a longitudinal compressive force of 1500kN during the optimization.

After the initial FE analysis high Von Mises stress levels where found around the windows adjacent to the door openings. The mesh was refined in these areas, and to further optimize weight reduction, multiple domains were utilized to appropriately distribute ply thickness were needed as illustrated in Figure 18.

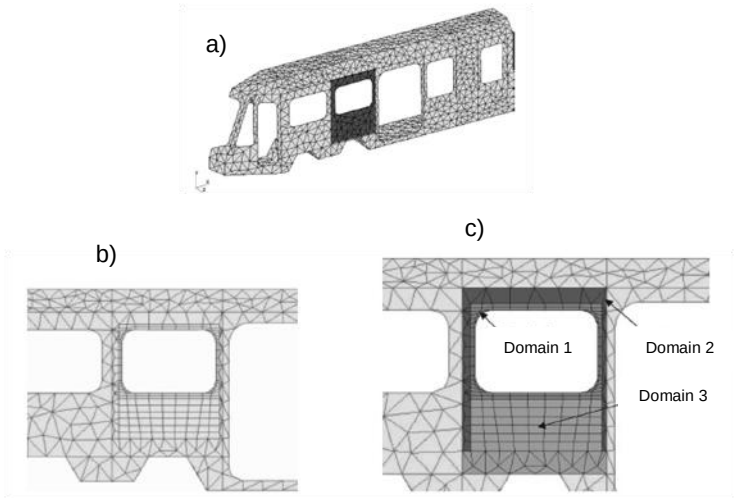

Figure 18, car body mesh illustrating the multi-level approach
a) original mesh, b) refined mesh around critical window panel, c) domain breakdown [7]

Young's Modulus	**Value [GPa]**
E_1	38.04
E_2	10.52
E_3	10.52
Shear Modulus	**Value [GPa]**
G_{12}	3.16
G_{13}	3.16
G_{23}	2.54
Poisson's ratio	**Value [-]**
v_{12}	0.285
v_{13}	0.285
v_{23}	0.284
Tensile strength	**Value [MPA]**
S_{t1}	820
S_{t2}	21.0
S_{t3}	21.0
Compressive strength	**Value [MPA]**
S_{c1}	491.0
S_{c2}	107.0
S_{c3}	107.0
Shear strength	**Value [MPa]**
S	40.0

Table 12, face sheet properties, subscript 1 = fibre direction, 2 = transverse direction, 3 = out of plane direction [7]

Young's modulus	**Value [MPa]**
E	21.5
Shear modulus	**Value [MPa]**
G	7.73
Poisson's ratio	**Value [-]**
v	0.39
Density	**Value [kg/m^3]**
ρ	60

Table 13, foam core properties [7]

It proved difficult to achieve the required safety margin around the window fillet with the above sandwich configuration. The optimized ply thicknesses around the window ended at 7.8mm, 6.1mm and 10.0mm (upper constraint) for the 0°, ±45° and 90° plies respectively. The author suggested instead that additional ply layers could be used in these areas. In other areas the ply thickness was significantly reduced down to the lower constraint of 0.25 mm. A weight reduction of 15% was achieved for the most critical panel (window panel) compared with the initial design. This implies that a weight reduction well above 15% should be possible over the entire car, sandwich to sandwich (!).

J. S. Kim et al. developed an expert system to calculate the optimum stiffness design of composite laminates for a train car body by varying the stacking sequence [17]. Optimal stiffness was achieved by quasi-isotropic stacking with design rules such as: avoid grouping of 90° plies, shield primary load carrying plies and do not differ ply angles between adjacent plies more than 45°. These design rules minimized the objective function for most loading situations, however, several other combinations showed good results with a lower number of plies compared to the quasi-isotropic stacking. During uniaxial loading cross-ply stacking was the stacking sequence that, not surprisingly, minimized the objective function.

K. B. Shin and S. H. Hahn studied how environmental ageing affects the structural integrity of the TTX car body [16], mainly by looking at how ageing effects influence the integrity of the composite skins. Tests showed severe decrease in stiffness and strength for the graphite/epoxy specimens except for the transverse tensile stiffness which showed an 8% increase over time due to post-curing effects. The transverse compressive stiffness and transverse tensile strength showed the largest decay over time, -17.5% and -27.74% respectively. The shear strength on the other hand remained relatively constant. By using an electron microscope the authors showed that the decay in strength and stiffness was most likely due to loss of matrix material from the surface of the composite specimens. FE analysis was performed on the car body, with both non-degraded and degraded mechanical properties. Interestingly the maximum stress levels in the composite structure with degraded properties were lower than in the case of non-degraded. The stress levels in the under frame slightly increased but were well within safety values. However, after degradation the car body's maximum deflection under vertical load had increased by about 8%, exceeding the prescribed limit.

P. Wennhage performed an optimisation investigation on a rail vehicle with acoustic and mechanical constraints [19]. The lowest natural frequency constraint was set to 9.5Hz and the car body was subjected to a compressive coupler load of 2000kN. Buckling of the floor was designated the most critical failure mode, why local and global buckling stresses of the floor sandwich panels where used as constraints during calculations. The sandwich panels where constructed of quasi-isotropic carbon fibre reinforced polymer laminates with a foam core. Face and core thickness as well as core density was used as design variables in the floor and mechanical properties of the core where calculated in the same manner as eq. (27) and (28). For the roof and side walls the core thickness and density was kept constant while the face thickness was the only design variable. An additional acoustic constraint on the sound reduction index was used on the floor. To make sure that approximations of sandwich characteristics, like the ones illustrated in Figure 8, are acceptable the face to core thickness ratio was used as an additional constraint. Two sandwich plates models where utilized in the simulation, a mechanical plate model and an acoustic plate model. The Method of Moving Asymptotes was employed for the structural-acoustic optimisation.

Simulations showed that both frequency and acoustic constraints strongly influenced the weight of the car body. An evaluation of the acoustics constraint's influence on the weight of the car body was done by removing this constraint, the weight of the car body was then lowered an additional 23% below the original optimization.

Siemens constructed the Combino, an end-to-end low floor tram vehicle designed for inner-city mass-transport. The car body of the Combino was comprised of a welded aluminium under frame and bolted aluminium sections for the body framework. Because of the low floor concept the motorised modules are mounted in containers on the roof. For this roof structure aluminium sandwich panels where utilised. Furthermore, the front of the tram is constructed by sandwich composites. The Combino was initially successful, but unexpected structural problems where encountered from torsional forces during curve negotiation. Information about this topic is scarce (some information can be found on Siemens website, c.f. address below*) and the references found are not fully reliable why this topic, for the moment, is left as so. However, it seems that Siemens eventually decided to replace the original COMBINO with the COMBINO plus, this time constructed of welded stainless steel.

**http://www.transportation.siemens.com/ts/en/pub/products/mt/products/tram/combino_history.htm*

5 Rail vehicle design criteria

Criteria presented in this section are summarizations of criteria found in European norm prEN 12663-1 [28] if no other specific reference is given. Criteria found in [28] are guidelines and detailed criteria are usually agreed upon between operator and supplier. These can either be stricter or more lenient than the ones presented herein. Design criteria also differ substantially between countries. While the norm studied here is a European norm, criteria in North America for example utilize up to 80% higher compressive forces during design verification, while the Japanese prescribe 3-4 times lower tensile and compressive loads for some rail vehicles. This can be justified by differing vehicle weights, e.g. North American freight trains typically have a five times higher weight than their European equivalent [27].

Design criteria presented below are for passenger vehicles, category P-II [28].

5.1 Vibration criteria

The running gear of a train interacts with the track to produce a periodic motion of typically a couple of cycles per second. Increased speed boosts these frequencies levels. To avoid passenger discomfort, or even structural damage, the car body should be designed with sufficient stiffness in the vertical, lateral and torsional directions. Also the interface between bogie and car body should be carefully examined. To avoid resonance the two structures should not display similar Eigen frequencies. In [32] a frequency separation flowchart is presented where bogie frequencies are in the range of 5-7Hz and Table 14 exemplifies some typical car body Eigen frequencies for a high speed train.

Mode direction	Frequency (first Eigen mode)
Vertical	9-10 Hz
Lateral	10-11 Hz
Torsional	11-12 Hz

Table 14, Eigen frequencies of a high speed train ($v \geq 200$ *km/h*) with good dynamic properties [27]

The lowest Eigen mode of the vehicle may be used as a stiffness requirement.

5.2 Load cases

Rail vehicle mass is split into three categories, mass of the car body, mass of running gear and payload mass, cf. Table 15. These masses are later used to define typical operational requirements.

Appellation	Description
m_1	Design mass of fully equipped vehicle body [kg]
m_2	Design mass of boogie or running gear [kg]
m_3	Normal design payload [kg]
m_4	Exceptional payload [kg]

Table 15, load case masses defined in [28]

A rail vehicle is subjected to a wide range of compressive, tensile, bending and twisting forces. To avoid permanent damage of the rail vehicle during operations it should be designed to withstand the following load cases. However, if technical justification is presented, either higher or lower values may be utilized instead of the ones presented herein.

5.2.1 Compressive and tensile forces

The compressive and tensile loads presented in Figure 19 are exceptional static loads which the car body should withstand whilst still sustaining a fully operational condition.

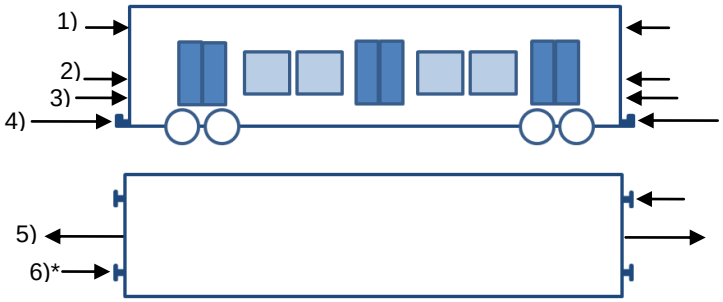

Figure 19, compressive and tensile forces for public transport vehicle, the corresponding forces are found in
Table 16
**not applied simultaneously with tensile force*

#	Applied at	Type	Magnitude
1)	End wall area, height of cant rail	compressive	300kN
2)	End wall area, height of waist rail	compressive	300kN
3)	End wall area, 150mm above top of structural floor	compressive	400kN
4)	Over couplers	compressive	1500kN
5)	Coupler area	tensile	1000kN
6)	Diagonally at buffer height	compressive	500kN

Table 16, forces defined in Figure 19, according to [28]

During all compressive and tensile tests above, a vertical load of $m_1 g$, cf. Table 15, should be applied.

5.2.2 Vertical loads

To prove structural integrity during exceptional operating conditions the car body is tested with the maximum payload defined as

$$F_z = 1.3 \cdot (m_1 + m_4) \cdot g \quad \textbf{(30)}$$

This load is uniformly distributed over the floor of the car body as shown in Figure 20.

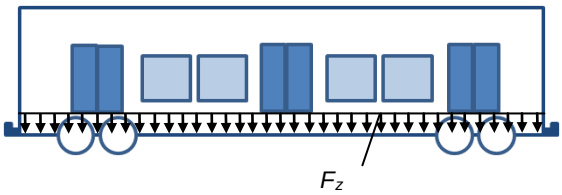

Figure 20, vertical load for public transport vehicle

5.2.3 Lift criteria

There are two different lifting criteria. The first is defined to illustrate a lift in a workshop. The rail vehicle is then raised via specified lifting points. An additional dynamic factor of 1.1g is applied and both boogies are left hanging under the car. The vertical load is then given by

$$F_z = 1.1 \cdot (m_1 + 2m_2) \cdot g \quad \textbf{(31)}$$

The second lifting case is for example after simple derailments of the rail vehicle were one of the boogies is still on track. During this lift the rare boogie (if it is the front boogie that has derailed) is on the track and the front of the vehicle is lifted, with the front boogie hanging under the car. Also here a dynamic contribution of 1.1g is applied and the vertical load is written as

$$F_z = 1.1 \cdot (m_1 + m_2) \cdot g \quad \textbf{(32)}$$

An offset lifting situation should also be considered. In this case one of the four lifting points in the first example is displaced vertically from the other three by 10mm. No permanent deformations should occur during any of these cases

5.2.4 Super positioning of static loads

To prove significant strength the loads 4 and 5 in Figure 19 should be tested in combination with a vertical load of

$$F_z = 1 \cdot (m_1 + m_4) \cdot g \quad \textbf{(33)}$$

5.2.5 Proof of attachments

All components in the vehicle should be tested to withstand the load cases presented in Table 17.

Acceleration	Magnitude
Longitudinal	*±3g*
Transverse	*±1g*
Vertical	*(1 ± c*)·g*

Table 17, accelerations on vehicle components, **c = 2 at the ends falling linearly to 0.5 at the vehicle centre*

5.2.6 Articulated vehicles

An articulated vehicle is affected by forces that arise from movement of the adjacent vehicles. Besides the cases of super positioning loads the articulation joints should withstand the following load cases

Longitudinal: $\pm 3g \cdot (m_1^* + n \cdot m_2)$, **(34)**

m_1 = design weight of the adjacent vehicle*
n = number of boogies connected to the adjacent vehicle

Transverse: $\pm 1g \cdot p \cdot m_1^*$ **(35)**

m_1 = design weight of the adjacent vehicle*
p = % of the design mass that is effectively supported by the articulation

Vertical: $1.3g \cdot (m_1 + m_4)$, **(36)**

in a worst case scenario the adjacent car body is assumed to be empty, i.e. 1.3g·m_1

The articulated joints also have to withstand certain moments and allow for sufficient rotation in curves and slopes. These rotations should be defined from the minimum curvature found on the track.

5.2.7 Fatigue criteria

All rail vehicles are subjected to a varying amount of dynamic loads, e.g. altering payload weights, aerodynamic loads from pressure differences, accelerations during start and stop, accelerations arising during curves or slopes in the track, etc. Altering payload verification may be of greatest concern in metro and rapid transit applications where the payload can change significantly between stops. For high speed vehicles track induced loading and aerodynamic loading are more critical.

[28] provides empirical vertical and lateral acceleration levels consistent with normal European operations that may be applicable if no other data is available. These track induced- and traction and breaking accelerations for passenger rolling stock are presented in Table 18.

Direction	Acceleration
Transverse	±0.15g
Vertical	(1±0.15)g
Longitudinal	±0.15g

Table 18, fatigue accelerations, 10^7 cycles

The structure should withstand these loads for 10^7 cycles. Appropriate combinations of the above load cases should also be considered to identify worst case scenarios.

Depending on the specific design route and operational speed significant aerodynamic loading may occur during trains passing, tunnel operations or exposure to high cross winds. It is

ultimately up to the operator and supplier to identify and examine all sources of cyclic loading which may cause fatigue damage.

5.3 Uncertainty factors

During the design stage of a railway vehicle (or any other vehicle, building, etc) it is important to take consideration to several uncertainty factors. These can arise from for example manufacturing processes which are rarely 100% accurate to design specifications, or the analytical accuracy of calculations which are commonly based on several approximations. These, and other, uncertainties may be allowed by applying safety factors during the design process in accordance with the operator. The following safety/uncertainty factors can be used as guidelines [28]. Other values may be chosen based on agreements between operator and supplier.

5.3.1 Yield or proof strength

$$\frac{R}{\sigma_c} \geq S_1 \qquad (37)$$

S_1 = safety factor
R = is the material yield or 0.2% proof strength in N/mm^2
σ_c = the calculated stress in N/mm^2

When design is only verified by calculations the safety factor S_1 should be 1.15.

5.3.2 Ultimate strength

$$\frac{R_m}{\sigma_c} \geq S_2 \qquad (38)$$

S_2 = safety factor
R_m = is the material ultimate stress in N/mm^2
σ_c = the calculated stress in N/mm^2

Typical value of S_2 = *1.5*. S_2 includes the uncertainty factor S_1.

5.3.3 Stability

$$\frac{\sigma_{cb}}{\sigma_c} \geq S_3 \qquad (39)$$

S_3 = safety factor
σ_{cb} = is the critical buckling stress in N/mm^2
σ_c = the calculated stress in N/mm^2

Typical value of S_3 = 1.5.

5.4 Sandwich construction

Critical features are commonly identified through supplier's experience together with structural analysis. This is one of the disadvantages with sandwich construction. Complete car bodies of sandwich structures are scarce, limiting the supplier's experience. Sandwich structures also have differing failure modes compared to more conventional structures, cf. Chap. 5.5. Consequently other safety factors may come into play when analysing sandwich structures, particularly when studying composite skins.

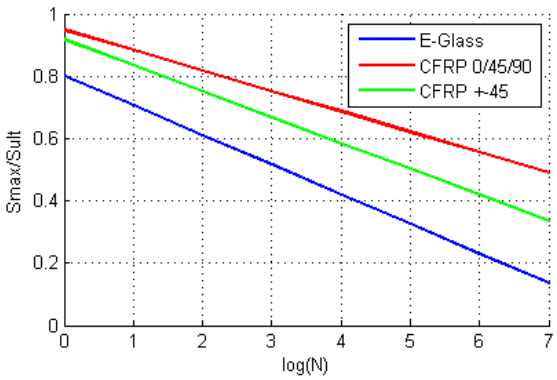

Figure 21, Conservative SN curves for 2 CRFP/epoxy and E-glass composites [29] in tension - tension. Curves represent a 95% lower bound confidence level.
Load frequencies:
E-glass < 5Hz, CFRP < 20Hz

A composite laminate will behave different when for example comparing a stress strain curve of a cross-ply laminate ([0° 90°]) with a [±45°] laminate, with respect to loading direction. The cross ply will likely exhibit a linear curve up to failure whereas the angle-ply curve will be highly non-linear from start to failure due to the contribution from the matrix.

In [23] the fatigue of E-glass and CFRP/epoxy composites for tension – tension tests was evaluated. Several conservative formula for SN curves for the individual materials and with varying fibre orientation where defined and three are presented in Figure 21. These are lower bound curves fit from tension - tension tests which seem to show that no fatigue limit, in contrary from steel, exists.

5.5 Failure modes of sandwich structures

Like most of the theory regarding sandwich structures in this study the following section contains summarizations of theory found in [2] if not indicated otherwise. As some derivations are quite extensive and rigorous they are left out of this literature study and the interested reader is referred to the given references. Furthermore, when studying composite laminates, the failure criteria may be very complex. These criteria are not covered here, but simply, according to [2], the criteria most commonly used for engineering analysis.

5.5.1 Face yielding/fracture

Depending on material selection the face sheet will have a maximum allowed stress level which, if exceed, results in yielding or fracture failure. Since with thin face sheets $\sigma_z = \tau_{xz} = \tau_{yz} = 0$, the maximum principal stress is given by Mohr´s circle of stress. For metallic faces it may be of interest to use a yield formula, e.g. Von Mises.

With regard to eq. (12) the failure criteria for a sandwich beam in bending may be reduced to

$$\bar{\sigma}_{fi} = \frac{M_i z E_{fi}}{D_i} \geq \hat{\sigma}_{fi} \qquad (40)$$

The superscript (^) represents the failure stress and (–) the maximum stress in the face. Here, and throughout this section, *i* is either the *x* or *y*-direction. For in plane loads the criteria is simply

$$\bar{\sigma}_{fi} \geq \hat{\sigma}_{fi} \qquad (41)$$

A corresponding failure for the core could also be defined, however, since the core usually has a much higher fracture or yield strain than the face sheet, the face sheets will likely be the first to fail.

5.5.2 Core shear failure

As mentioned, the major stresses in the core are shear stresses, however, the direct stresses in the core are not always negligible why the core shear failure criteria becomes

$$\bar{\tau}_{ciz} = \left[\left(\frac{\sigma_{ci}}{2}\right)^2 + \tau_{ciz}^2\right]^{\frac{1}{2}} \geq \hat{\tau}_{ciz} \qquad (42)$$

Once again *i* is either the *x* or *y*-direction.

With a weak core, $E_c << E_f$, the direct stress influence vanishes, and in agreement with eq. (19) for a weak core, the shear criteria can be approximated to

$$\bar{\tau}_{ciz} = \frac{T_i}{d} \geq \hat{\tau}_{ciz} \qquad (43)$$

5.5.3 General buckling

As for non-sandwich structures it is important to avoid buckling of the panels since when buckled the panel may lose its entire load carrying capabilities. The main difference when studying buckling of sandwich beams or plates compared with solid beams or plates is that one must account for the shear deformation. The critical buckling load, P_{cr}, can be expressed as

Figure 22, buckling of a sandwich beam

$$\frac{1}{P_{cr}} = \frac{1}{P_b} + \frac{1}{P_s} \qquad (44)$$

where P_b is the buckling load due to bending and P_s is the shear buckling load. This formula is derived from the concept of partial deflection, which states that the total deflection w of a beam or plate can be expressed as

$$w = w_b + w_s \qquad (45)$$

Here w_b and w_s are partial deflections due to bending and shear deformation respectively. The different buckling loads can be derived from energy equations for the beam or plate, e.g. minimizing the potential energy. P_b can usually be found in handbooks while P_s can be calculated or, for beams, set equal to the shear stiffness S.

If post buckling loading continues the beam will eventually fail. This failure will be of type compressive/tensile failure of the skin, face wrinkling or core shear fracture (“shear crimp”).

5.5.4 Face wrinkling/local buckling

Face wrinkling is one of the few failure modes where the transverse normal stiffness of the core has an important influence. There are two types of face wrinkling, symmetric and anti-symmetric wrinkling, cf. Figure 23.

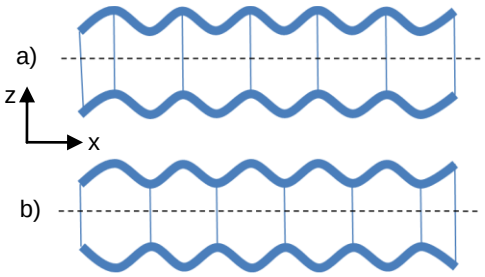

Figure 23, face wrinkling.
a) Anti-symmetric, b) symmetric

Face wrinkling is a form of local, short wave, buckling of the faces. The displacements are quickly damped out through the thickness of the core, assuming that the core is of sufficient thickness. Failure can occur in two ways, if the compressive strength of the core is lower than the tensile strength of the core and the adhesive joint an inward wrinkle can arise. The opposite is that a wrinkle causes a tensile fracture of the core or the adhesive joint.

A common, conservative, formula for calculating the critical stress for face wrinkling in the design of sandwich construction is given in eq. (46). This equation can be applied to continuously supported, relatively smooth and isotropic faces, e.g. foam core sandwich structures.

$$\sigma_{fi,cr} = 0.5 \cdot \sqrt[3]{E_{fi} \cdot E_{ci} \cdot G_{ci}} \qquad (46)$$

The above formula is derived for plane stress, for sandwich panels a state of plane strain predominates. In this case the E modulus in eq. (46) may be altered to $E/(1-\nu^2)$. It is also of importance to apply the correct modulus in the above equation, e.g. when studying composite skins. The face modulus, E_{fi}, should be the bending stiffness modulus whilst the core modulus, E_{ci} and G_{ci}, are those of out of plane stresses, cf. Figure 23.

In a more practical application, during multi axial loading, the principal stresses are calculated in which case the critical face wrinkling stress should also be calculated for the same directions as they may differ significantly, for example when using multidirectional laminates for skin material. If both principal stresses are compressive some sort of interaction formula may be necessary to evaluate the integrity of the structure.

For highly anisotropic faces the critical wrinkling stress will vary strongly with in-plane direction in which case the critical stress may first be reached in a direction different from the principal stresses. This is due to the fact that the principal stresses do not coincide with the principle strains for highly anisotropic laminates.

Other, less conservative, formula and consequences of face wrinkling and the related stresses can be found in [2].

5.5.5 Face dimpling

Face dimpling is similar to face wrinkling but effects non-continuously supported skins, e.g. honeycomb or corrugated cores when the wavelength of the wrinkles is less than that of the unsupported area. An empirical formula for the critical face dimpling stress for hexagonal honeycomb cores is given in eq. (47).

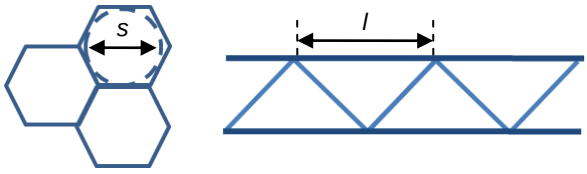

Figure 24, example of length s in a honeycomb core and length l in a corrugated core

$$\sigma_{f,cr} = \frac{2E_f}{1-\nu_f^2}\left(\frac{t_f}{s}\right)^2 \qquad (47)$$

For corrugated cores the critical face dimpling stress takes the form

$$\sigma_{f,cr} = \frac{k\pi^2 E_f}{12\left(1-\nu_f^2\right)}\left(\frac{t_f}{l}\right)^2 \qquad (48)$$

The variables s in eq. (47) and l in eq. (48) are illustrated in Figure 24. k in eq. (48) is the buckling coefficient and depends on the size of the plate.

5.5.6 Shear crimp

Shear crimp failure is illustrated in Figure 25. This failure is common in a post buckled state where the transverse forces reach a maximum. The critical stress is given by

Figure 25, shear crimp failure of a sandwich beam

$$\sigma_{fi} = \frac{S_i}{2t_{fi}} \quad (49)$$

5.5.7 Local indentation/impact

The ideal load transfer for a sandwich structure is as mentioned when the core is loaded in a state of pure shear and the faces are loaded in a membrane state of stress. During localized loading or impact the sandwich is subjected to non-optimum loads which can result in bending or shear failure of the faces, compressive failure of the core or delaminating of the face and core. When looking at FRP faces further failure modes arise such as fibre tensile or compressive failure, shear failure of the matrix material, etc. A local failure of the above mentioned kind can later propagate to affect the integrity of the entire panel. A mayor problem is that the effects of localized loads or indentations may not be visible from the outside of the panel, for example delamination or core compressive failure.

In [31] local indentation or loads are divided into three categories, large and small mass indentations, and indentations that fall in between these two categories. For small mass indentations the panel response is dominated by buckling and shear waves which arise during impact. For large mass indentation a quasi-static response arises. The response type can be predicted by checking the ratio between the mass of the indenter, M_i, and the mass of the maximum affected panel area M_{pmax}.

According to [31] small mass indentation response will arise if

$$\frac{M_i}{M_{pmax}} < \frac{1}{4} \quad (50)$$

and large mass indentation response if

$$\frac{M_i}{M_{pmax}} > 2 \quad (51)$$

Complex responses come up between these two cases, where by more advanced FE-analysis may be required in comparison to the analytical solutions presented in [31]. However, in the two well defined cases, the maximum forces are given followed by several failure criteria. According to [31] crushing of the core material, when studying rigid cores, is the first and most common failure mode. The critical force for core compressive failure, F_{cr}, is given by

$$F_{cr} = 8\hat{\sigma}_{cz}\sqrt{\frac{D_f^* t_c}{1.38 Q_{zc}^*}}, \quad t_c \leq t_{c\,max} \tag{52}$$

$$F_{cr} = 8\hat{\sigma}_{cz}\sqrt{\frac{2 t_{c\,max} D_f^*}{Q_{zc}^*}}, \quad t_c > t_{c\,max} \tag{53}$$

where D_f^* is the effective flexural rigidity of the face and is for isotropic face sheets given below, as well as the thickness $t_{c\,max}$.

$$D_f^* = \frac{E_f t_f^3}{12\left(1 - v_f^2\right)} \qquad t_{c\,max} = t_f \frac{32}{27}\left(\frac{4Q_f^*}{3Q_{zc}^*}\right)^{\frac{1}{3}} \tag{54}, \tag{55}$$

Q_{zc}^* is the effective transverse stiffness of the core and may be approximated by the elasticity modulus E_c. In eq. (55) Q_f^* is the effective stiffness of the face and is as follows

$$Q_f^* = \frac{12 D_f^*}{t_f^3} \tag{56}$$

Further more, the indenter is assumed to be of spherical geometry. Other failure forces defined in [31] are for example matrix fracture and delaminating of the face forces.

A simple design criteria for local loads around for example fittings and joints, is presented in [35] and is purely

$$A = \frac{P}{\hat{\sigma}_{cz}} \tag{57}$$

This equation gives a conservative estimation of the minimum needed area, *A*, over which the load *P* can be applied without core compressive/tensile failure seeing as no regard is taken to the properties of the face sheet which will always give some transverse resistance.

5.5.8 Debonding

The adhesive bond between face and core may fracture if the stress in the joint exceeds the adhesive strength. However, it seems as if this failure mode is often omitted due to its complexity and the fact that sandwich structures commonly utilise adhesives strong enough so as not to become one of the first failure modes. Debonding can still occur via crack propagation originating in a small (or large) flaw in the adhesive joint leading to the conclusion that debonding failure is rather a manufacturing problem than a design problem. In [35] three out of 124 beams tested until failure in three point bending failed by debonding. The authors concluded that these beams had significant defects introduced in the adhesive joint during manufacturing and that if care is taken during manufacturing debonding is unlikely to occur.

Formulas, such as face wrinkling and face dimpling critical stresses, are derived for a perfect face. However, due to non-perfect manufacturing processes etc., face sheets commonly have some sort of small local imperfections. Because of this the actual failure stresses are smaller than the ones derived above why it is important to thoroughly evaluate safety factors that coincide to, among other things, the manufacturing precision and estimations of material properties that are common when considering sandwich structures.

It may not be of interest to evaluate safety factors and design criteria for all failure modes, but simply the failure modes which are likely to occur first for the applied load case. For example tensile or compressive yield of the core is often omitted since, as mentioned, the materials used in the faces often have a lower yield or fracture strain. It is still of importance to realise all failure modes. The core compressive failure may not be of interest when studying global loads, but it is the most likely failure mode when considering local loads or indentations.

To get better control over the failure mode of a sandwich structure it can be designed to fail in a particular fashion. This is done by first identifying the three sets of variables that define a failure mode; loading variables, material properties and sandwich geometry. For chosen materials and a given loading case one can now with the failure modes defined above determine how different geometry variables influence the first failure mode. This is done by calculating the transition curves between the different failure modes, i.e. setting the failure loads for the different modes equal to one another. This method can be found in several papers, e.g. [2], [35] and [36], and the result is a failure mode map like the one illustrated in Figure 26.

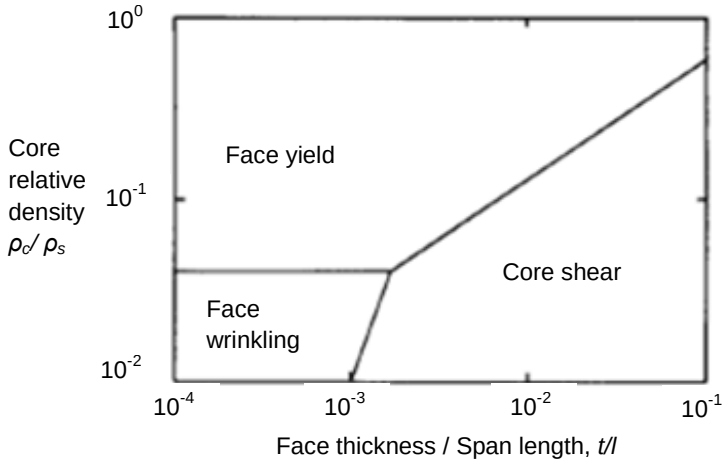

Figure 26, failure mode map for a sandwich beam with aluminium face sheets and a foam core [35].

The relative density is the quota between the apparent density of the foamed core, ρ_c and the density of the un-foamed solid of which the core material is made, ρ_s. Span length l is simply the length of the beam.

Other areas that should be taken into consideration are for example fire, collision, and projectile impact (“windscreen criteria”) safety.

6 Bus design criteria

Rail vehicle have a high tare weight per passenger in comparison to other transportation modes, e.g. the weight per seat is three times higher for the X2000 in comparison to a NEOPLAN Spaceliner N117 bus [19]. It would therefore be interesting to compare design criteria between busses and rail carriages to evaluate the reason/reasons for this discrepancy. However, when going through the literature, (such as Regulation No. 66 of the Economic Commission for Europe of the United Nations [40]), only a few design criteria have been found. Most commonly the rollover criterion is mentioned, for example ECE reg. 66 only covers rollover. This design criterion is summarised below.

6.1 ECE Regulation 66

Design criteria and guidelines here are summarized from Regulation No. 66 of the Economic Commission for Europe of the United Nations (UNECE) [40]. Regulation 66 is for approval of large passenger vehicles with regard to the strength of their superstructure. The superstructure is defined as

> *"...the load bearing components of the bodywork as defined by the manufacturer, containing those coherent parts and elements which contribute to the strength and energy absorbing capability of the bodywork, and preserves the residual space in the rollover test"* [40]

The residual space is defined as

> *"...a space to be preserved in the passengers', crew and driver's compartment(s) to provide better survival possibility for passengers, driver and crew in case of a rollover accident"* [40]

The residual space is calculated by creating a vertical plane perpendicular to the longitudinal direction of the bus and then moving this plane throughout the length of the bus, with some small exceptions at the end and beginning, as shown in Figure 27.

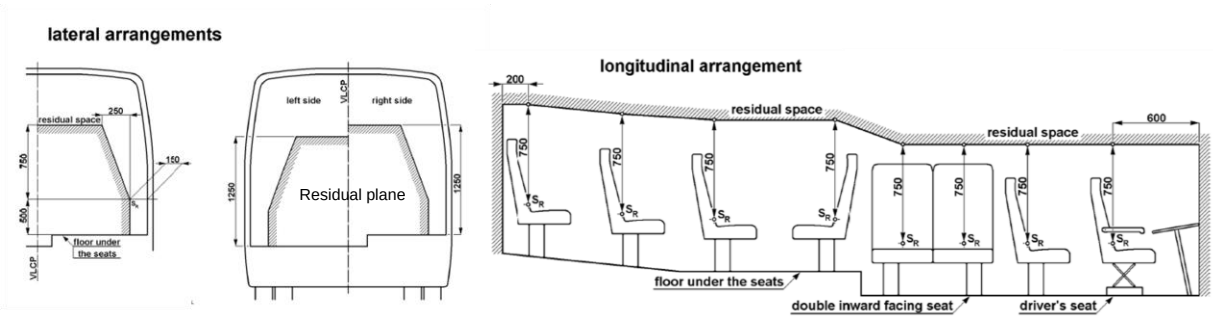

Figure 27, residual space as defined in ECE Reg. 66 [40]. To the left, the lateral arrangement, depicting the vertical residual plane within the shaded border, to the right the vertical plane is extended throughout the length of the vehicle to make up the residual space.

In [40] the masses of the vehicle are divided into the four groups presented in the Table 19 below.

Mass	Notation	Description
Unladen kerb mass	M_k	The mass of the vehicle in running order, unoccupied and unladen but with an additional mass of 75kg for the driver.
Total occupant mass	M_m	The combined mass of all passengers and crew who occupy seats with occupant restraints.
Total effective vehicle mass	M_t	M_k + ½ M_m
Individual occupant mass	M_{mi}	The mass of an individual occupant. This mass is set to 68kg

Table 19, classification of masses for passenger vehicles [40]

During a rollover the residual space must be kept in tacked. The total energy that must be absorbed by the super structure is calculated as the difference in potential energy of the centre of gravity before and after the rollover event as

$$E_T = 0.75Mg\Delta h = 0.75Mg(h_1 - h_2) \quad \textbf{(58)}$$

Where $M = M_k$ if no occupant restraints are available, otherwise $M = M_t$. The variable Δh is defined as the difference between the vertical height of the centre of gravity of the vehicle from its most unstable equilibrium position, h_1, i.e. just before the vehicle begins to roll, cf. Figure 28, and the height of the centre of gravity when the bus has rolled over, h_2. The rollover test is furthermore performed at the edge of a ditch of depth 0.8m, thus increasing the height of the fall. The constant 0.75 is used to deal with the dissipation of energy into the ground through, for example, vibration.

Other than this it is mainly impact response that is studied for bus design. In [41] Haibin Ning et al. study the impact response of sandwich panels subjected to a static load of 8896N applied by a pad not larger than 3225.8mm^2, which, according to the authors, is a procurement guideline from the American Public Transport Association. This load is applied to all exterior body panels below the rub rail (~below windows) of the vehicle.

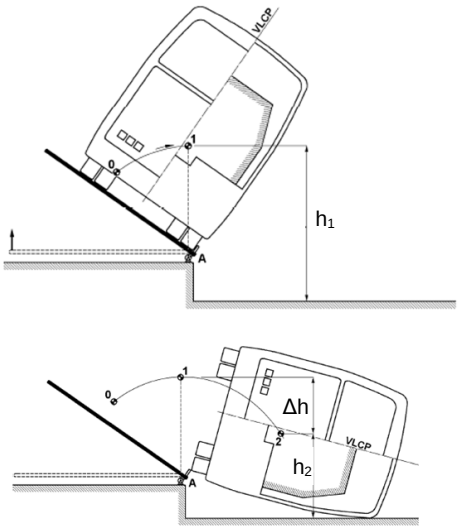

Figure 28, rollover event [40], notice that the bus is allowed to deform as long as the residual space is kept in tacked.

6.2 Support placement

Another interesting, yet crude, comparison can be made between rail and bus vehicles if one looks at the wheel/bogie placements. If we simplify the bus and train to beam shapes with wheels and bogies simplified to simple supports, we can make a quick comparison of the reaction forces that affect the vehicles. For this I have chosen the bus type NEOPLAN Spaceliner N117/3 [43], and the high-speed train X2000 middle car UB2. The model of the bus and train is depicted in Figure 29, and corresponding dimensions can be found in Table 20.

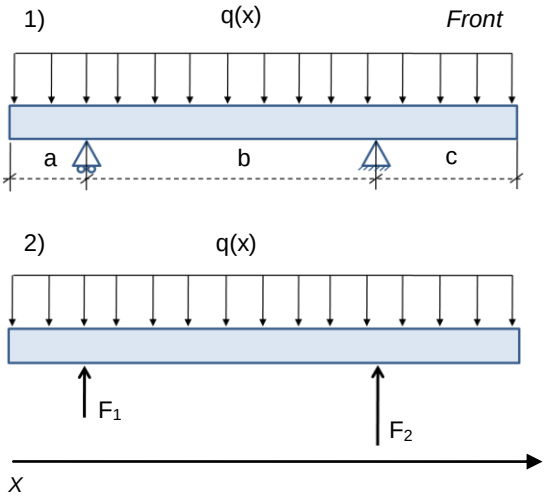

Figure 29, crude vehicle model with uniform load q(x), 1) simple supported model, 2) exposed model

To further simplify things let us assume that the weight of the vehicles is evenly distributed by the force *q(x)* [N/m], and that this load is the same for both vehicles, further more the lengths of the two vehicles is set to unity so that the only difference between the two models is the support placements, i.e. the relative lengths *a*, *b* and *c*.

Properties	Neoplan Spaceliner N117/3 [43]	X2000 mid car*
a [m]	3.25	3.35
b [m]	6.05	17.7
c [m]	2.87	3.35
Empty weight [kg]	25500	48000
Number of seats	55	76

Table 20, dimensions, weight and number of seats in the Spaceliner and X2000, dimensions corresponding to the lengths in Figure 29. **courtesy of Bombardier Transportation, mid car UB2 which has a relatively large number of seats in comparison to other X2000 mid cars*

The reaction forces in the two vehicles are shown in Figure 30. Here one can see that the relative support placements of the X2000 induce greater reaction forces than for the support placements of the Spaceliner. In fact, if the Spaceliner would have supports at the same relative position as the X2000, the maximum transverse force would increase by almost 36% and the maximum bending moment would increase nearly 60%, as illustrated in Figure 30.

In Figure 31 the actual lengths are used and the load distributing force *q(x)* is the same for both vehicles, i.e. assuming they can carry the same amount of passengers, seats, etc, per unit of length. This results in that the total force acting on the X2000 is about twice as large as that on the Spaceliner (since the X2000 car is almost exactly twice as long). From Figure 31 it is clear that, with regard to all the above assumptions and simplifications, the X2000 car has to withstand a maximum transverse force that is 170% larger than that of the Spaceliner and a 530% larger bending moment.

By optimising the placement of the supports on the X2000 car, the maximum bending moment can be reduced by 60% in comparison to the current value in this example (this placements is calculated by setting the magnitude of the maximum negative and positive bending moments

equal to one and another, which results in *a = c = 20.71% of total length,* a plot of these forces can be found in the appendix, Figure 34.

There are, however, other factors to take into consideration when looking at bogie placement, for example curve negotiation and effects from adjacent vehicles. When placing the bogies closer to one another the rail vehicle goes from hanging over the inside of the curve with the mid part of the car, to sticking out further on the outside with the front and rear of the car. This induces greater movement between the coupled cars, thus increasing the requirements on the coupling. Furthermore, no matter how good the coupling is, this will undoubtedly inconvenience the passage between cars.

A more suiting comparison may be to look at an articulated bus, which do have a shorter overhang towards the rear of the front car, however, the relatively large overhang at the front, in relation to total length, plus the fact that the trailer commonly only has one set of running gear close to the centre of the trailer, still gives the bus better support placement.

Another reason for the tare weight per seat discrepancy between rail vehicles and buses is that rail vehicles typically offer larger passenger areas per seat than busses. For train travel over 100km the area per seat is in the range 1.0 - 1.1m^2 in 2nd class (1.4 - 1.6m^2 in 1st class) whilst passenger area in buses is around 0.6m^2 per seat [27].

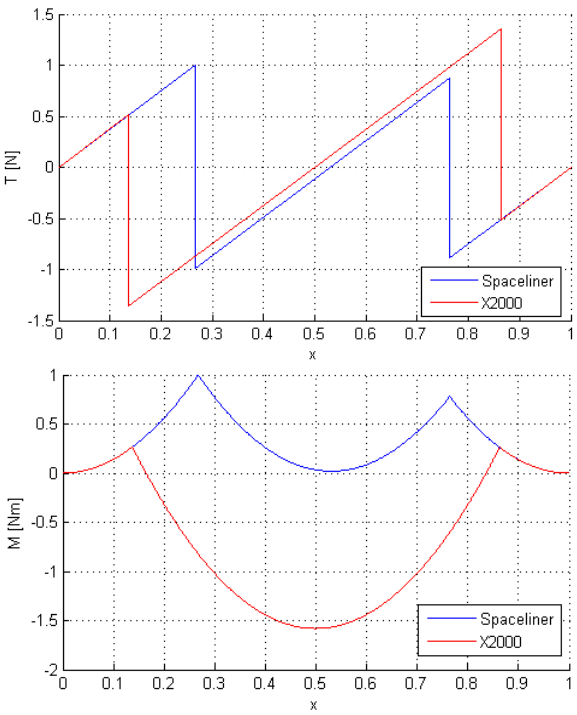

Figure 30, transverse force T and bending moment M calculated from reactions forces from supports on the X2000 and Spaceliner according to Figure 29. Forces are normalised with respect to maximum forces in the Spaceliner. Lengths of the vehicles are equal in this comparison.

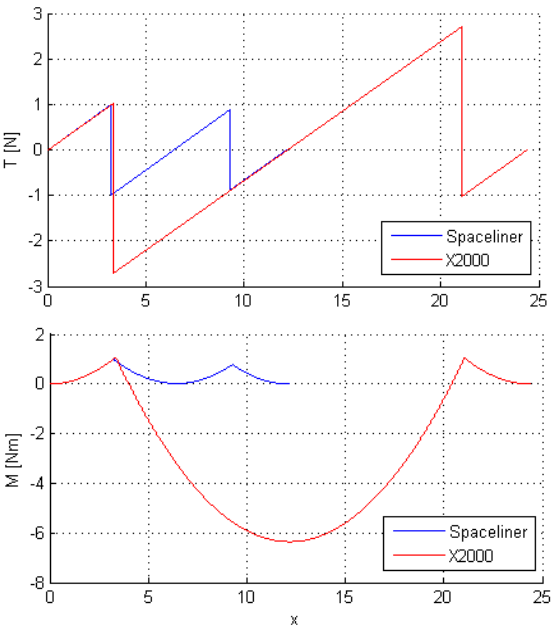

Figure 31, transverse force T and bending moment M calculated from reactions forces from supports on the X2000 and Spaceliner according to Figure 29. Forces are normalised with respect to maximum forces in the Spaceliner

7 Conclusions

It seems as if sandwich design would significantly lower the mass of any structure, and it is easy to get blindsided by its apparent potential. Care should, however, be taken as when quickly summarising the rail vehicles presented herein, all but one, the Schindler wagon [10], have utilized reinforcing steel frames within the body structure.

Difficulty of accurately modelling sandwich components also seems to be an issue. Interestingly the TTX finite element analysis showed higher natural frequencies than those measured during tests, whilst Bombardier's C20 FICA demonstrated the opposite characteristics. A comparison of modelling techniques would be interesting. Common practice is to assume a perfect bond between face and core in the sandwich panel, thus enabling 2-dimensional plate modelling with effective material properties. Even though this may be a good approximation, FE-analysis should for this reason show a stiffer car body than reality.

The test done on the TTX in [12], [14] and [15], and optimizations in [7] suggest that sufficient strength can be provided by a sandwich structure with composite skins. The main concern is the stiffness of the car body which was improved by inserting steel frames.

Changing window and/or door configuration so that stresses do not congregate around sharp cut-outs and allow forces to propagate straighter through the structure may be an alternative solution to steel frame stiffeners. However, door openings in particular, have to be of certain width and height to allow convenient access in and out of the rail vehicle.

Most vehicles found have been constructed with a thicker outer face (when considering composites the outer face has often been twice as thick). The reasons for this may be several although the one that stands out is better impact protection.

An aspect that has not been touched throughout this study is the cost of the different solutions. This boundary condition is likely one of the most pressing when finally settling on a sandwich design.

Bus design criteria specified in chap. 6.1 do not help in finding the reason for the mass discrepancy between rail and other public transport vehicles. However, certain guesses can be made, for example rail vehicles are guided, and thus a strong body is needed to withstand induced forces from the track. Rail vehicles travel at higher speeds, higher speed requires stronger and stiffer vehicles to withstand larger forces. Furthermore, because of the large (larger than bus) transverse forces and bending moments subjected to the X2000 car, cf. chap. 6.2, it is not surprising that a great deal of steel is used for the construction of the vehicle, thus making it a relatively heavy transportation vehicle.

8 References

[1] J R Vinson, “Sandwich structures: Past, Present and Future”, Proceedings of the 7th International conference on Sandwich Structures

[2] D Zenkert, “An Introduction to Sandwich Structures”, Student edition

[3] G Wihlborg, “Hållfasthetslära”, Lunds Universitet 2004, 3rd edition

[4] S I Seo, J S Kim and S H Cho, “Development of a hybrid composite body shell for tilting trains”, Proceedings of the Institution of Mechanical Engineers; Part F; Journal of rail and rapid transit

[5] Hexel Composites, “HexWeb™ Honeycomb sandwich design technology”, Publication No. AGU 075b, December 2000

[6] S H Kim, S G Kang, C G Kim and K B Shin, “Analysis of the Composite Structure of Tilting Train Express (TTX)”

[7] A H Harte, J F McNamara and I D Robby, “A multilevel approach to the optimisation of a composite light rail vehicle body shell”, Composite Structures, Vol. 63, Issues 3-4, 2004 pp 447-453

[8] K F Karlsson and B T Åström, “Manufacturing and applications of structural sandwich components”, Composites Part A: Applied Science and Manufacturing, Vol. 28, Issue 2, 1997, pp 97-111

[9] K Prince, “Composites track down rail opportunities”, Reinforced Plastics, Volume 45, Issue 6, June 2001, pp 50-51

[10] Anonymous, “Schindler is on track with FRP trains”, Reinforced plastics, November 1995, pp 28-32

[11] G Marsh, “Prepregs –raw material for high-performance composites”, Reinforced Plastics, Volume 46, Issue 10, October 2002, pp 24-28

[12] J S Kim, J C Jeong, “Natural frequency evaluation of a composite train car body with length of 23m”, Composites Science and Technology, Volume 66, Issue 13, October 2006, pp 2272-2283

[13] R Stewart, “At the core of lightweight composites”, Reinforced Plastics, Volume 53, Issue 4, April 2009, pp 30-35

[14] J S Kim, S J Lee, K B Shin, “Manufacturing and structural safety evaluation of a composite train car body” Composite Structures, Volume 78, Issue 4, June 2007, pp 468-476

[15] J S Kim, J C Jeong, S J Lee, “Numerical and experimental studies on the deformational behavior a composite train carbody of the Korean tilting train”, Composite Structures, Volume 81, Issue 2, November 2007, pp 168-175

[16] K B Shin, S H Hahn, “Evaluation of the structural integrity of hybrid railway carriage structures including the ageing effects of composite materials”, Composite Structures, Volume 68, Issue 2, April 2005, pp 129-137

[17] J S Kim, N P Kim, S H Han, “Optimal stiffness design of composite laminates for a train carbody by an expert system and enumeration method”, Composite Structures, Volume 68, Issue 2, April 2005, pp 147-156

[18] G Belingardi, M P Cavatorta, R Duella, “Material characterization of a composite–foam sandwich for the front structure of a high speed train”, Composite Structures, Volume 61, Issues 1-2, July 2003, pp 13-25

[19] P Wennhage, “Structural – Acoustic Optimization of sandwich Panels”, Doctoral Thesis Report 2001

[20] http://www.plascore.com/

[21] http://www.diabgroup.com/
[22] http://www.matweb.com/
[23] http://www.hexcel.com/
[24] http://www.rohacell.com/
[25] http://www.DOW.com/
[26] D B Miracle, S L Donaldson, “Technology Overview”, ASM Handbook online, Volume 21, Composites, Introduction to Composites
[27] E Andersson, M Berg, “Spårtrafiksystem och spårfordon, Del 2: Spårfordon”, Railway Group KTH, Div. of Railway Technology, Dep. of Aeronautical & Vehicle Eng, the Royal Institute of Technology 2007
[28] CEN, “Railway applications – Structural requirements of railway vehicle bodies – Part 1: Railway vehicles other than freight wagons”, prEN 12663-1, May 2007
[29] C E Demers, “Fatigue strength degradation of E-glass FRP composites and carbon FRP composites”, Construction and Building Materials, Volume 12, Issue 5, 1 July 1998, pp 311-318
[30] Bombardier Transportation, “C20FICA Measurement of Natural Frequencies on B Carbody”, Internal doc. 3EST000215-0102
[31] R Juntikka, “Dimensionering för punktbelastning” 2008 SICOMP AB
[32] E Andersson, M Berg, S Stichel, “Rail Vehicle Dynamics”, Railway Group KTH, Div. of Railway Technology, Dep. of Aeronautical & Vehicle Eng, the Royal Institute of Technology 2005
[33] Bombardier Transportation, “Final stress analysis report”, Internal doc. 3EST000205-3371
[34] R Juntikka, R Lundström, “Punktbelastning – Jämförelse mellan beräkning och provning”, 2008 SICOMP AB
[35] T C Traintafillou, L J Gibson, “Failure Mode Maps for Foam Core Sandwich Beams”, Materials Science and Engineering, Volume 95, November 1987, pp 37-53
[36] A Petras, M P F Sutcliffe, “Failure mode maps for honeycomb sandwich panels**”,** Composite Structures, Volume 44, Issue 4, April 1999, pp 237-252
[37] Oskar Fröidh, “Perspectives for a future high-speed train in the Swedish domestic travel market”, Journal of Transport Geography, Volume 16, Issue 4, July 2008, pp 268-277
[38] K B Shin, J Y Lee, S H Cho, “An experimental study of low-velocity impact responses of sandwich panels for Korean low floor bus**”,** Composite Structures, Volume 84, Issue 3, July 2008, pp 228-240
[39] http://etran.fiber-x.com/
[40] UNECE Regulation No 66, “Uniform technical prescriptions considering the approval of large passenger vehicles with regard to the strength of their superstructure”
[41] Haibin Ning, Gregg M. Janowski, Uday K. Vaidya, George Husman, “Thermoplastic sandwich structure design and manufacturing for the body panel of mass transit vehicle” Composite Structures, Volume 80, Issue 1, September 2007, pp 82-91
[42] B L Nelldal, “Möjligheter för tåget att konkurrera med och ersätta flyget”, Railway Group, Dep. of traffic and logistics, the Royal Institute of Technology, February 2007
[43] http://www.neoplan.info/

9 Appendix

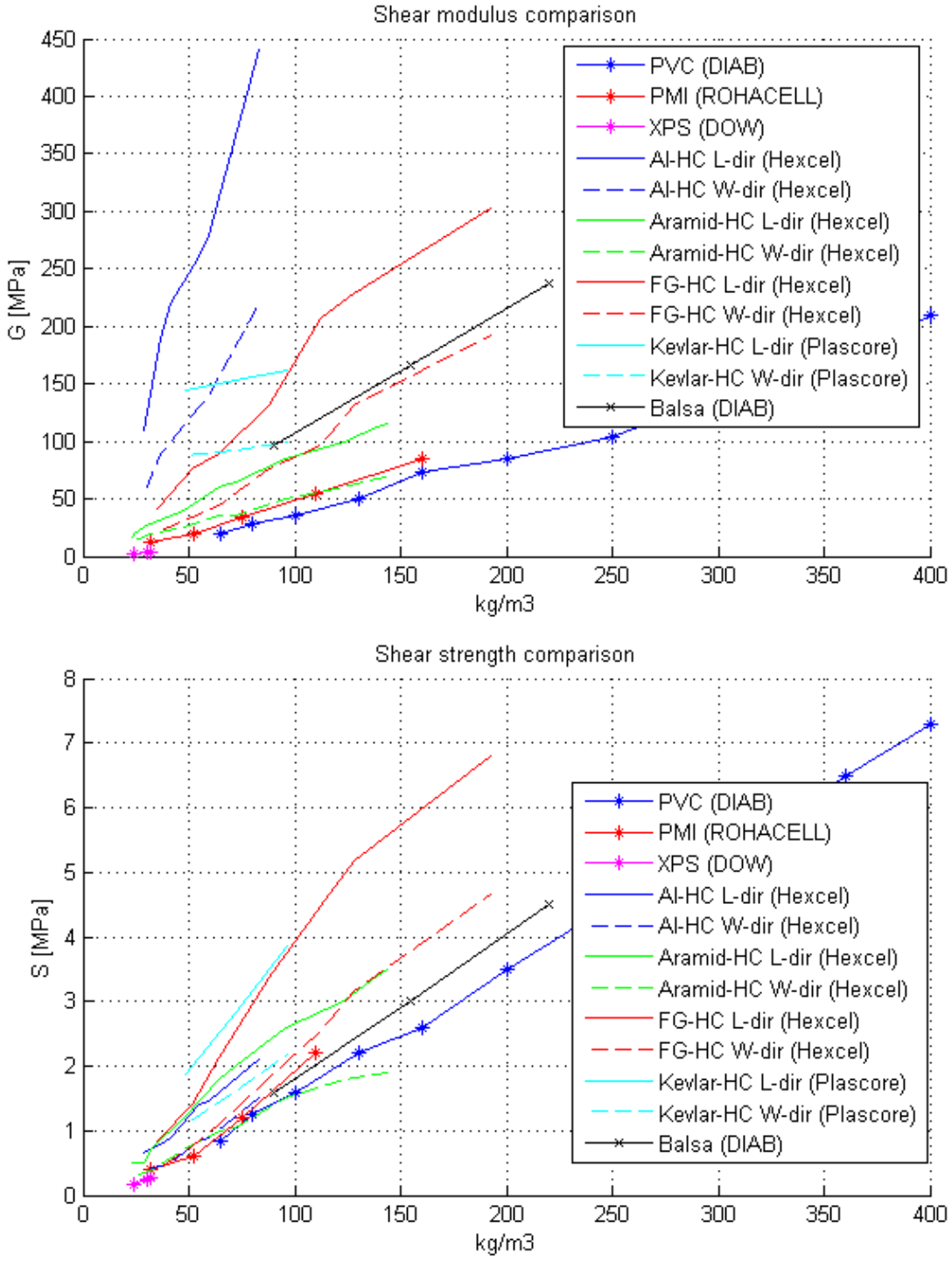

Figure 32, Comparison of core shear properties, top: shear modulus, bottom: shear strength
HC = honeycomb, Al = aluminium, FG = fibreglass, XPS = extruded polystyrene
Plascore's values from Higher Shear configuration honeycomb

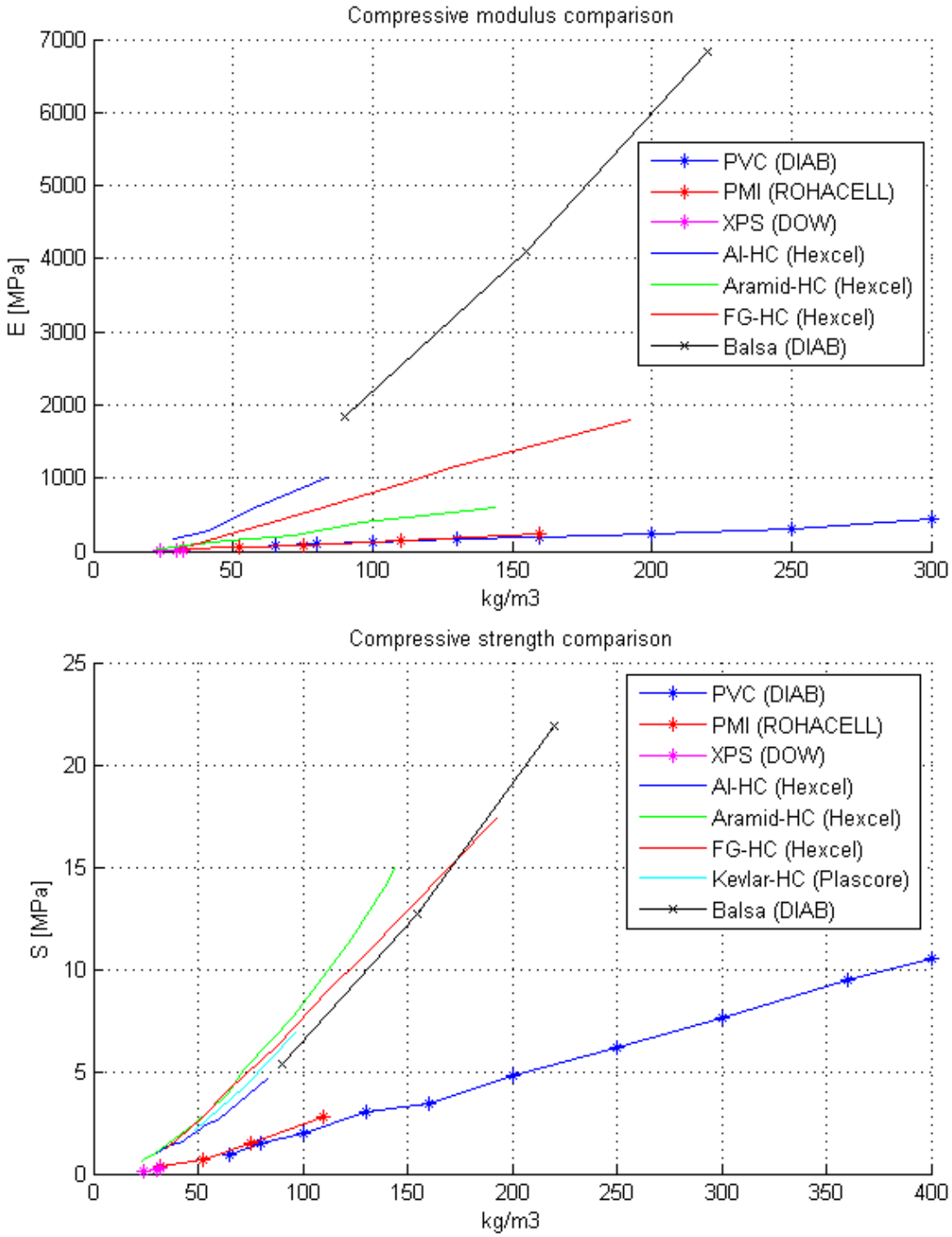

Figure 33, Comparison of out of plane compressive core properties, top: compressive modulus, bottom: compressive strength

HC = honeycomb, Al = aluminium, FG = fibreglass, XPS = extruded polystyrene

***OBS**: Compressive modulus for Rohacell PMI not actually a compressive modulus but according to Röhm a Modulus of elasticity evaluated from a tensile type test*

Compressive modulus for DOW EPS not actually compressive modulus but a flexural modulus

Compressive modulus not found for Plascore Kevlar honeycomb

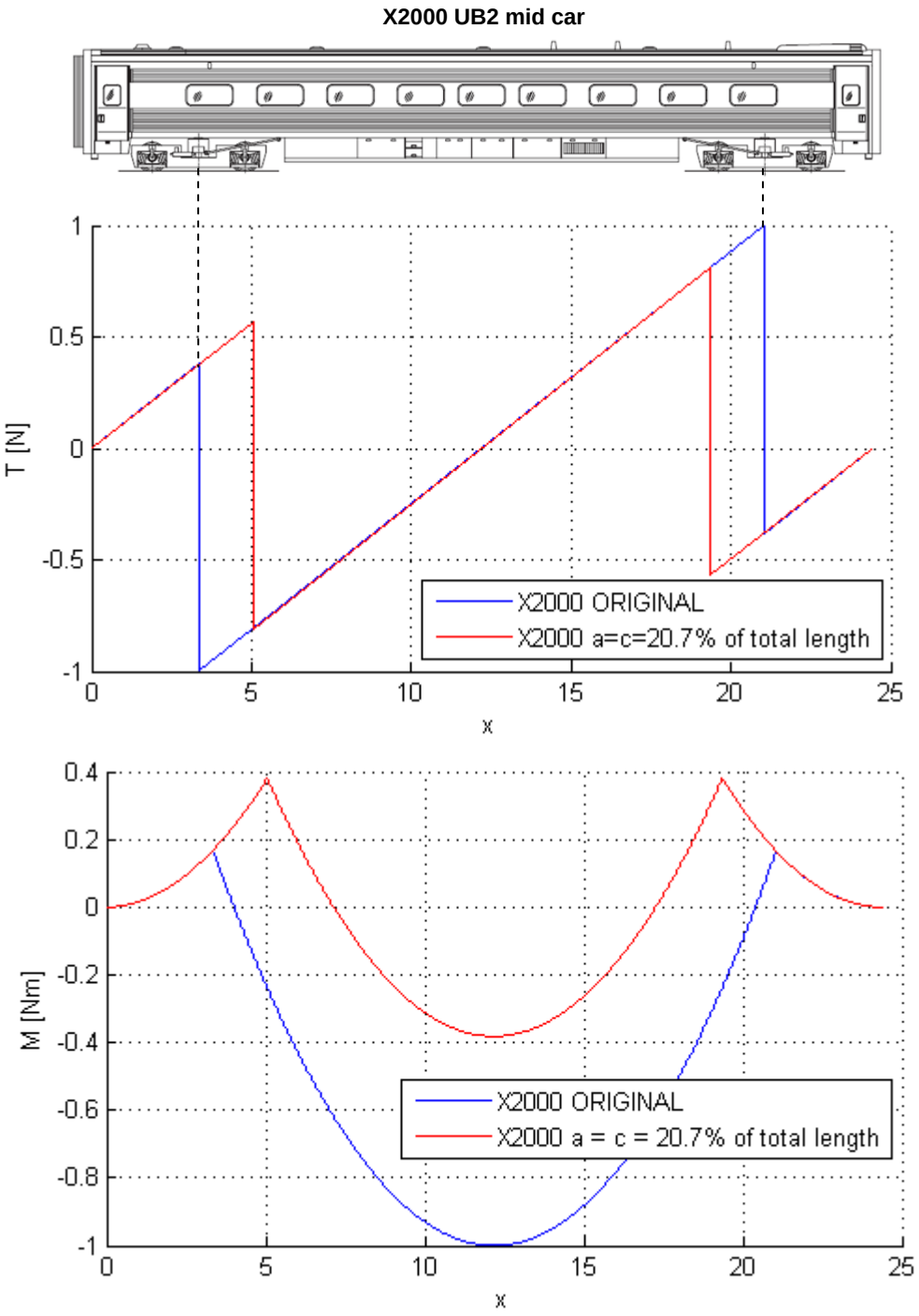

Figure 34, comparison of reaction forces between original bogie placement and optimal bogie placement on the X2000 UB2 mid car, cf. Figure 29, assuming evenly distributed load over the rail car. Normalised forces and moments with regard to the maximum values found in the original X2000 configuration.
Illustration of X2000 mid car courtesy of Bombardier Transportation